Still Competitive: Revisiting Recurrent Models for Irregular Time Series Prediction

Anonymous authors
Paper under double-blind review

Abstract

Modeling irregularly sampled multivariate time series is a persistent challenge in domains like healthcare and sensor networks. While recent works have explored a variety of complex learning architectures to solve the prediction problems for irregularly sampled time series, it remains unclear what are the true benefits of some of these architectures, and whether clever modifications of simpler and more efficient RNN-based algorithms are still competitive, i.e. they are on par with or even superior to these methods. In this work, we propose and study GRUwE: Gated Recurrent Unit with Exponential basis functions, that builds upon RNN-based architectures for observations made at irregular times. GRUwE supports both regression-based and event-based predictions in continuous time. GRUwE works by maintaining a Markov state representation of the time series that updates with the arrival of irregular observations. The Markov state update relies on two reset mechanisms: (i) observation-triggered reset, and (ii) time-triggered reset of the GRU state using learnable exponential decays, to support the predictions in continuous time. Our empirical evaluations across several real-world benchmarks on next-observation and next-event prediction tasks demonstrate that GRUwE can indeed achieve competitive to superior performance compared to the recent state-of-the-art (SOTA) methods. Thanks to its simplicity, GRUwE offers compelling advantages: it is easy to implement, requires minimal hyper-parameter tuning efforts, and significantly reduces the computational overhead in the online deployment.

1 Introduction

Multivariate time series and their models are critical for understanding and analyzing real-world dynamical systems. While traditional time-series models assume that the observations are made at regular time intervals, real-world data, such as healthcare records or sensor readings, are often irregularly sampled. In other words, events or measurements associated with these events may occur at different times and in different contexts (e.g., special lab tests in clinical settings may occur only during patient crises). The key challenge here is to devise the models of time series that are able to accurately capture the dependencies among individual variables and events occurring at different times from the observed data. We study this important problem in the context of time series prediction (forecasting) and event prediction tasks.

A variety of models ranging from classic statistical and modern deep learning frameworks have been developed to support time-series prediction task for irregular settings. Early approaches replaced the irregularly observed data with regularly spaced observations by inferring their values at the regular time points. Classic statistical auto-regressive models (AR, ARMA, ARIMA) Shumway & Stoffer (2017) or latent space models, such as, Linear Dynamical Systems (LDS) Kalman (1963) models could then be applied to support prediction at future regular times. To support prediction on arbitrary future prediction times, various smoothing and interpolation methods were deployed. More recently, classic time-series models have been gradually replaced with various types of modern neural architectures capable of handling irregularly sampled observations Siami-Namini et al. (2018). The existing methods include extensions of *RNN approaches* Che et al. (2018); Mei & Eisner (2017), and continue with *differential equation approaches* Rubanova et al. (2019); De Brouwer et al. (2019); Chen et al. (2018); Schirmer et al. (2022); Becker et al. (2019), *attention-based approaches* Shukla & Marlin (2021); Chen et al. (2023), *graph-based approaches* Zhang et al. (2022; 2024); Yalavarthi et al. (2024) and *state-space modeling approaches* Smith et al. (2023); Gu & Dao (2023).

Recent work on irregular multivariate time series has largely gravitated toward increasingly complex architectures: continuous-time neural ODEs Rubanova et al. (2019); Kidger et al. (2020); Chen et al. (2023), transformers Zuo et al. (2020); Zhang et al. (2020); Shukla & Marlin (2021); Yang et al. (2022), and graph-based models Zhang et al. (2024); Yalavarthi et al. (2024); Li et al. (2025); Luo et al. (2025). These new modeling mechanisms and their combinations may however come with intricate training pipelines due to more number of hyper-parameters or higher sensitivity to them, inductive biases that are difficult to interpret or analyze, and substantial computational overhead. These factors may limit their benefits in many realistic settings: training datasets with a limited size or resource-constrained environments (e.g., bedside monitoring systems, embedded clinical devices) where the efficiency of inference is critical for their deployment. Design objectives have historically prioritized model sophistication over practical runtime considerations. This raises a natural question: *could carefully designed, simple models that are rooted in simpler architectures, still achieve comparable or even superior predictive performance at significantly lower computational cost?* We investigate this question by proposing **GRUwE** (Gated Recurrent Unit with Exponential basis functions), pronounced as "groovy", a relatively simple yet effective GRU-based architecture that maintains the Markov state representation of the multivariate process that is updated at irregular observation times. GRUwE models the effect of time with the help of learnable exponential basis functions. State updates are affected by both: (i) the arrival of new observations, and (ii) the elapsed time since the previous observation. This dual mechanism allows the model to naturally accommodate influence of past observations and irregular time intervals between them. To make predictions at an arbitrary future time, GRUwE reuses the same exponential basis functions that are used for state updates. Our extensive experiments comparing GRUwE against the SOTA baselines lead to better or comparable predictive performance with significantly lower computational costs.

While the proposed GRUwE model supports continuous-time prediction at future time points, its architecture naturally extends to event prediction setting through Temporal Point Process (TPP) framework. We can formulate a Conditional Intensity Function (CIF), that represents an instantaneous rate of event arrival for a TPP by applying a SoftPlus non-linearity at the output of the GRUwE's regression function. Our experiments demonstrate that GRUwE-based event prediction matches or outperforms state-of-the-art CIF-based TPP models, including: *RNN models* Du et al. (2016); Mei & Eisner (2017), *attention-based models* Zhang et al. (2020); Zuo et al. (2020); Yang et al. (2022) and *differential equation models* Chen et al. (2020).

The main contributions of this work are:

- We propose GRUwE, an irregular time series model, that maintains a Markov state representation, defines two reset state update mechanisms to capture dependencies inherent in multivariate time series and supports continuous-time inference.
- We perform a comprehensive evaluation of GRUwE against SOTA prediction models on next observation prediction and next event prediction tasks on multiple real-world datasets. Our evaluation reveals that GRUwE performs competitively on both the tasks, while achieving new SOTA on 2 datasets on the next observation prediction, and achieving the highest overall rank in the next event prediction task.
- We demonstrate that GRUwE's compact Markov state representation leads to substantial improvements in computational efficiency during online deployment of irregular time series models.

2 Related Work

In this section, we review existing work on time series prediction for irregularly sampled time series data and contrast them to the proposed GRUwE model.

RNN approaches exploit efficient sequential hidden-state updates for prediction, with the hidden state serving as a compact, Markovian summary of all past observations. Classical RNN models assume regularly sampled time series and therefore require interpolation schemes to handle irregularly sampled data. Several extensions adapt recurrent models to continuous time by updating the hidden state only at observation times, including Recurrent Marked Temporal Point Processes (RMTPP) Du et al. (2016), GRU-D Che et al. (2018), FullyNN Omi et al. (2019), and the Neural Hawkes Process (NHP) Mei & Eisner (2017). RMTPP extends classic RNN architecture by adding a parametric conditional intensity function that predicts the distribution of the next event time directly from the RNN's hidden state. NHP, based on LSTM Hochreiter

& Schmidhuber (1997) architecture, uses exponential decays to a predicted target cell state to derive a continuous-time cell state representation, which is eventually used to represent the intensity function to model time-varying intensities and complex temporal point-process dynamics. GRU-D extends GRU by explicitly modeling missingness and irregular sampling using learnable decay mechanisms that impute both inputs and hidden states based on the time since each variable was last observed. Missing observations are inferred in GRU-D using decay mechanisms that revert to a target value, typically determined by the mean value of the variable. The GRU-D and GRUwE models are similar in their use of the exponential decay functions for modeling the effect of elapsed time on the hidden state. However, GRU-D uses decay functions to infer missing observation values. As a result, it may propagate estimation errors for missing observations in time. In contrast, GRUwE does not interpolate missing observations and uses exponential decay function to directly model latent variable trajectories both for the state update and prediction module.

Differential Equation approaches offers another widely-used approach to model multivariate time series and their dependencies in continuous time. Differential Equation (DE) models rely on differential equations models of latent space dynamics. Neural ODE Chen et al. (2018) defines temporal dynamics in continuous time in terms of ordinary differential equations (ODEs) approximated by a learned dynamics model. Rubanova et al. (2019) proposes to combine this Neural ODE dynamics with VAE-like architectures (referred to as LatentODE) and RNN architectures (known as ODE-RNN) to model irregularly sampled time series. One limitation of Neural ODEs is that its solution is a function of the initial condition, however, the initial condition cannot be adapted to the observed distribution. Neural Controlled Differential Equations Kidger et al. (2020); De Brouwer et al. (2019) allows the dynamics to be continuously modulated by including the input observations. The differential equation methods typically require an external numerical ODE solver, a component that can significantly increase model's training time. Recently, Schirmer et al. (2022); Becker et al. (2019) avoid invoking numerical solvers for continuous-time dynamics by modeling latent transitions with the help of linear stochastic differential equations, that can be solved in the closed form. In contrast to the above DE methods, GRUwE relies on a set of learnable exponential decay functions to represent the latent state dynamics. GRUwE avoids the need for deployment of computationally costly external numerical solvers.

Alternative approaches. A range of recent methods move beyond recurrent models to address prediction under irregular sampling. These approaches differ in how they represent time, model dependencies, and handle the lack of regularly spaced inputs, leading to several different modeling paradigms. **Temporal attention** methods eliminate the need to approximate a latent Markov state and instead learn prediction functions directly from the observed inputs. Models such as mTAND Shukla & Marlin (2021), THP Zuo et al. (2020), SAHP Zhang et al. (2020), A-NHP Yang et al. (2022) embeds time into fixed-size learnable vectors and learn relationship between irregular observations and prediction timepoints in continuous time. ContiFormer Chen et al. (2023) combines Neural ODEs with the continuous-time attention mechanism to model irregular observations. **GNN Approaches.** Many of the recently proposed irregular time series models rely on Graph Neural Networks (GNN). T-PatchGNN Zhang et al. (2024) uses a patch-based mechanism on univariate time series to enhance local feature extraction and use graph neural network to learn relationships among different time series. GraFITi Yalavarthi et al. (2024) first converts irregular samples to a special bipartite graph structure and cast the prediction problem as an edge weight prediction. HyperIMTSLi et al. (2025) improves on the GraFITi method by replacing its fixed bipartite graph with a learnable, heterogeneous hypergraph that jointly models variable–time relations, enables richer message passing, and produces more expressive irregular time series representations. Other graph-based temporal Zhang et al. (2022), spatiotemporal Marisca et al. (2022) and diffusion-based Tashiro et al. (2021) models have been proposed to address irregularly spaced observations. Overall, the main difference between the above models and GRUwE is a Markov state representation that enables efficient update and deployment of our models in real-time settings supporting sequential prediction tasks. Typically the above transformer and graph-based models require one to buffer sequences of past observations to encode a newly arrived observation and reprocess all the past observations for every inference step from scratch which may become a computational bottleneck when sequences of past observation become very long. In contrast, GRUwE updates its state using only the previous state and the newly arrived observation, making it simple, efficient, and practical for real-time deployment.

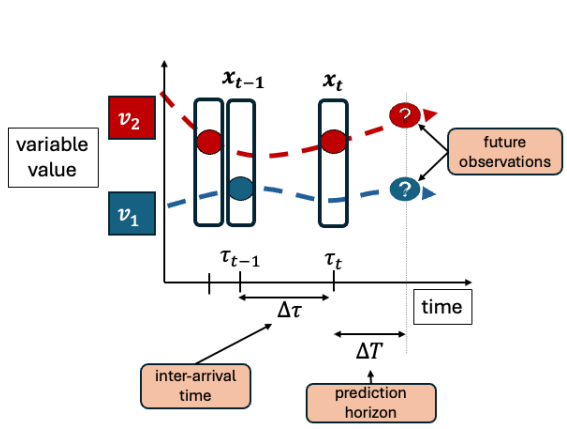

(a) Abstract diagram of the next-observation prediction problem for irregular time series. The true continuous dynamics function of the variables $\{v_1, v_2\}$ (dotted line) are unknown; the model only sees their values at irregular time points to formulate future predictions.

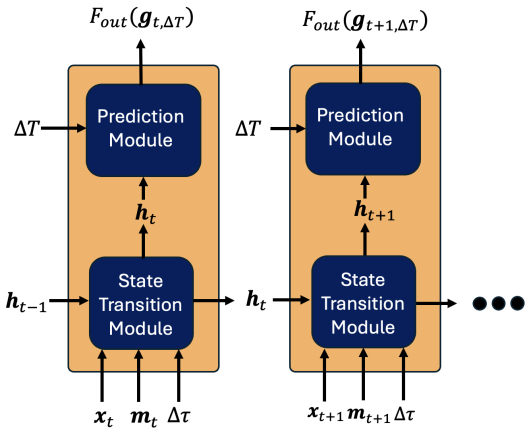

(b) GRUwE's overall architecture. At each observation time point, $\{\mathbf{x}_t, \mathbf{m}_t, \Delta\tau\}$ are processed to updated the previous hidden state ($\mathbf{h}_{t-1} \rightarrow \mathbf{h}_t$). The prediction module make a prediction using the hidden state $\mathbf{h}_t$ and prediction horizon ΔT.

Figure 1: Description of the problem and overview of the model architecture.

3 Problem Setting

Our goal is to model D-dimensional multivariate time series with irregularly spaced observations. For clarity, consider the case $D = 2$ with variables v_1 and v_2, whose latent temporal dynamics are illustrated as dotted trajectories in Figure 1a. The underlying generative process governing these variables is unknown. Observations occur at non-uniform time points (shown as dots), and may not be synchronized across variables; for instance, v_1 may be missing when v_2 is observed. At each time step $t \in \mathbb{Z}$ (corresponding to continuous time $\tau_t \in \mathbb{R}$), we define an input vector $\mathbf{x}_t \in \mathbb{R}^D$ where observed entries contain values and unobserved entries are masked. The time elapsed between successive observation times, also known as inter-arrival time, is denoted by $\Delta\tau = (\tau_t - \tau_{t-1}) \in \mathbb{R}_+$. To support prediction at any future time, we define a prediction horizon $\Delta T \in \mathbb{R}_+$, representing how far ahead (relative to τ_t) the prediction should be made. In the *next observation prediction* task, the model generates a predicted observation vector $\hat{\mathbf{x}}_{t,\Delta T}$ at time $\tau_t + \Delta T$, conditioned on the history of all observations up to time step t. In the *next event prediction* setting, the TPP model outputs event intensities $\lambda(\tau_t + \Delta T)$, given the event history up to time step t.

4 GRUwE: Gated Recurrent Unit with Exponential Basis Functions

Our goal is to define and learn a prediction model $f(\mathbf{x}_{1:t}, \boldsymbol{\tau}_{1:t}, \Delta T)$ that takes a history of a D-dimensional multivariate time series $\mathbf{x}_{1:t}$ made at times $\boldsymbol{\tau}_{1:t}$ respectively, and predicts future values of time series at time $\tau_t + \Delta T$.

Markov State. Since the observation history keeps growing in time, we approximate it with a fixed-size state model $\mathcal{H}_t$ that summarizes what is known about the process at time-step t. If $\mathcal{H}_t$ accurately summarizes the history of observations, it becomes Markov, making the past sequences independent of the future. A benefit of this is that the new state (after a new observation arrives) can be obtained by a state-update function which is a function of just the previous state and the new observation. This greatly simplifies the application and maintenance of the models for real-time (online) deployment. The state $\mathcal{H}_t$ of our GRUwE model consists of a latent vector $\mathbf{h}_t$ representing dependencies among different time series variables and their values. Thus, $\mathcal{H}_t = \{\mathbf{h}_t\}$ at time τ_t summarizes all the observation made until time t.

State Transition Module. As new observations arrive in time, the state model $\mathcal{H}_t$ representing the information seen so far, is updated with new observations. GRUwE's state transition model consists of two complementary reset mechanisms. The first accounts for the time elapsed since the previous observation with the help of a time-triggered reset mechanism. This is followed by an observation-triggered reset mechanism

to incorporate the influence of current input observation. In the following, we describe the design of reset mechanisms in more detail.

Time-Triggered Reset Mechanism. We model the effect of time elapsed in GRUwE with the help of time-triggered reset mechanism. Briefly, the time-triggered reset relies on a set of learnable exponential decay functions that take the previous hidden state vector, and the time difference between the previous and the new observation. The learnable exponential decay function for the hidden state vector is defined as:

$$\boldsymbol{\gamma}(\boldsymbol{\Delta\tau}) = \exp\{-\max(\mathbf{0}, \mathbf{W}_\gamma \boldsymbol{\Delta\tau} + \mathbf{b}_\gamma)\},$$

where $\boldsymbol{\Delta\tau}$ is the time elapsed vector indicating time-interval between two consecutive time indices: $(\tau_t - \tau_{t-1}) \cdot \mathbb{1}$; where $\mathbb{1}$ is a vector containing all 1s. The learnable parameters $\mathbf{W}_\gamma, \mathbf{b}_\gamma$ govern by how much each component of hidden state needs to be decayed before it is updated by the GRU cell:

$$\mathbf{g}_{t-1,\Delta\tau} = \boldsymbol{\gamma}(\boldsymbol{\Delta\tau}) \odot \mathbf{h}_{t-1}. \tag{1}$$

Observation-Triggered Reset Mechanism. When a new observation arrives at an irregular interval, GRUwE updates its state components with the help of observation-triggered reset mechanism. The input (new observation) at each time-step t is defined by an input vector $\mathbf{x}_t$ and a mask vector $\mathbf{m}_t$ indicating if an individual variable i is observed at time-step t:

$$m_{t,i} = \begin{cases} 1, & \text{if } \ x_{t,i} \ \text{ is observed} \quad (2) \\ 0, & \text{otherwise} \quad (3) \end{cases}$$

Since observations for multivariate times series may arrive at different times, the values missing in the inputs are masked. That is, at each time-step, the recurrent unit takes two vectors as the input: 1) a mask vector ($\mathbf{m}_t$) and 2) input vector ($\mathbf{x}_t$) where missing values are substituted with zeros:

$$\mathbf{x}'_t = \mathbf{m}_t \odot \mathbf{x}_t, \tag{4}$$

where, $\odot$ denotes the element-wise product.

Computing the hidden state ($\mathbf{h}_t$) at τ_t, given $\mathbf{g}_t$, $\mathbf{m}_t$ and $\mathbf{x}_t$ involves a set of updates similar to the ones found in the standard GRU unit:

$$\begin{aligned}
\mathbf{z}_t &= \sigma(\mathbf{W}_z \mathbf{x}'_t + \mathbf{U}_z \mathbf{g}_{t-1,\Delta\tau} + \mathbf{V}_z \mathbf{m}_t + \mathbf{b}_z), \\
\mathbf{r}_t &= \sigma(\mathbf{W}_r \mathbf{x}'_t + \mathbf{U}_r \mathbf{g}_{t-1,\Delta\tau} + \mathbf{V}_r \mathbf{m}_t + \mathbf{b}_r), \\
\tilde{\mathbf{h}}_t &= \tanh(\mathbf{W}_h \mathbf{x}'_t + \mathbf{U}_h (\mathbf{r}_t \odot \mathbf{g}_{t-1,\Delta\tau}) + \mathbf{V}_h \mathbf{m}_t + \mathbf{b}), \\
\mathbf{h}_t &= (1 - \mathbf{z}_t) \odot \mathbf{g}_{t-1,\Delta\tau} + \mathbf{z}_t \odot \tilde{\mathbf{h}}_t.
\end{aligned}$$

Note that $\mathbf{W}$s, $\mathbf{U}$s, $\mathbf{V}$s and $\mathbf{b}$s are learnable parameters of the model. The parameters let us fit the hidden state component and observations so that the dependencies among time series most important for the prediction are captured.

Prediction module. Our main goal is to be able to predict future values in continuous time domain, from past observation sequence. At each time step t, we rely only on the information encoded in the model's state $\mathcal{H}_t$ to support prediction. To enable flexible prediction across arbitrary future time points, we introduce a prediction horizon $\Delta T \in \mathbb{R}_+$, which specifies how far ahead in time (from the current time τ_t) the prediction should be made. The prediction module in GRUwE estimates the future output at time $\tau_t + \Delta T$ by conditioning on the Markov state $\mathcal{H}_t$ at time τ_t. It operates in two stages: (i) modeling the evolution of the Markov state up to the target time $\tau_t + \Delta T$ in continuous time, and (ii) Decoding the predicted values at that future time using a task-specific output function. For the evolution of Markov state in the prediction module, one can perhaps use a specialized continuous-time function different from the time-triggering reset used for modeling continuous dynamics between observations. However, for simplicity, GRUwE shares the exponential basis functions to model the dynamics of Markov state in the prediction module:

$$\boldsymbol{\gamma}(\boldsymbol{\Delta T}) = \exp\{-\max(\mathbf{0}, \mathbf{W}_\gamma \boldsymbol{\Delta T} + \mathbf{b}_\gamma)\}, \tag{5}$$

$$\mathbf{g}_{t,\Delta T} = \boldsymbol{\gamma}(\boldsymbol{\Delta T}) \odot \mathbf{h}_t. \tag{6}$$

The prediction module applies task-specific output function (for e.g., linear projection for prediction; intensity function for TPP) denoted by $F_{out}(\cdot)$, to decode the value at prediction horizon (ΔT):

$$\widehat{\mathbf{x}}_{t,\Delta T} = F_{out}(\mathbf{g}_{t,\Delta T}). \tag{7}$$

For the next observation prediction, the output function can be parameterized using linear projection or more complex Multi-Layer Perceptron (MLP). For simplicity, in our experiments, we use the linear projection specified using parameters $\{\mathbf{W}_{out}, \mathbf{b}_{out}\}$ as the $F_{out}(\cdot)$:

$$\widehat{\mathbf{x}}_{t,\Delta T} = \mathbf{W}_{out}\ \mathbf{g}_{t,\Delta T} + \mathbf{b}_{out}. \tag{8}$$

For the next event prediction, we use GRUwE's decayed hidden state ($\mathbf{g}_{t,\Delta T}$) to formulate the Conditional Intensity Function (CIF) for event type k at time $\tau_t + \Delta T$ as:

$$\lambda(\tau_t + \Delta T \mid \mathbf{h}_t, k) = \text{Softplus}(\mathbf{w}_\lambda^k\ \mathbf{g}_{t,\Delta T} + b_\lambda^k). \tag{9}$$

Here, the linear projection parameters $\mathbf{w}_\lambda^k$ and b_λ^k are the parameters of the CIF model specific to event type k. We apply the Softplus non-linearity to ensure that the output is positive, as intensity represents the instantaneous rate of event arrivals.

Summary of GRUwE. Our proposed model GRUwE, is a latent state transition model that maintains a Markov state of the process in continuous time to summarize the historical events. GRUwE primarily consists of a state transition module and a prediction module. To update its Markov state, the state transition module defines: i) time-triggered reset mechanism to account for the time-elapsed, and ii) observation-triggered reset mechanism to incorporate the influence of the observations. GRUwE's prediction module reuses the exponential basis function (used to model inter-arrival times) to support continuous-time prediction module. For more clarity, Figure 1b illustrates the process of sequentially feeding observation and mask vectors along with the time elapses for each time step, followed by a state transition module, to update the previous state as a function of current inputs. Ultimately, prediction module generates a prediction at a future time ΔT with the help of the updated state.

5 Analysis of Exponential Basis Functions

We theoretically analyze the properties and inductive biases introduced by the proposed exponential basis functions for modeling the temporal dynamics.

Asymptotic Behavior. We analyze the asymptotic behavior of the exponential basis function $\boldsymbol{\gamma}(\Delta T) = \exp\{-\max(\mathbf{0}, \mathbf{W}_\gamma \Delta T + \mathbf{b}_\gamma)\}$ and its effect on the decayed state $\mathbf{g}_{t,\Delta T} = \boldsymbol{\gamma}(\Delta T) \odot \mathbf{h}_t$. Consider the component-wise behavior for dimension i as $\Delta T \to \infty$:

Case 1: $W_{\gamma,i} > 0$ **(State Reset)**

- **Behavior:** $g_{t,\Delta T,i} \to 0$
- **Explanation:** When $W_{\gamma,i} > 0$, the argument $W_{\gamma,i}\Delta T + b_{\gamma,i} \to \infty$ as ΔT increases. As a result:

$$\max(0, W_{\gamma,i}\Delta T + b_{\gamma,i}) \to \infty \quad \Rightarrow \quad \exp(-\infty) \to 0.$$

Case 2: $W_{\gamma,i} = 0$ **(Constant Decay)**

- **Behavior:** $g_{t,\Delta T,i} \to \exp(-\max(0, b_{\gamma,i})) \cdot h_{t,i}$
- **Explanation:** With zero weight, the decay term simplifies to a constant:

$$\boldsymbol{\gamma}_i(\Delta T) = \exp(-\max(0, b_{\gamma,i})).$$

This results in a constant decay of the hidden state component. The final value depends on the bias term $b_{\gamma,i}$:

- If $b_{\gamma,i} \leq 0$: $\exp(-\max(0, b_{\gamma,i})) = \exp(0) = 1$ (no decay).
- If $b_{\gamma,i} > 0$: $\exp(-\max(0, b_{\gamma,i})) = \exp(-b_{\gamma,i}) < 1$ (constant decay).

Case 3: $W_{\gamma,i} < 0$ **(No Decay)**

- **Behavior:** $g_{t,\Delta T,i} \to h_{t,i}$
- **Explanation:** For negative weights, the decay rate $W_{\gamma,i}\Delta T + b_{\gamma,i} \to -\infty$:

$$\max(0, W_{\gamma,i}\Delta T + b_{\gamma,i}) \to 0 \quad \Rightarrow \quad \exp(0) = 1.$$

Asymptotic analysis reveals that the proposed exponential basis functions have three operating modes to express the latent temporal dynamics for each hidden component. Based on the learned value of the parameter $\mathbf{W}_\gamma$, the decay mechanism can either decay to zeros, perform constant decay, or no decay at all. The no decay mode can be used to *remember* the hidden state components indefinitely as time passes. This mechanism can be used to capture very long-term dependencies. The constant-decay mode is useful to capture dependencies that relies on counts, or perhaps when the inter-arrival times are approximately regularly spaced (since the decay is independent of time-elapsed ΔT). When $\mathbf{W}_\gamma > 0$, the exponential basis functions decay with increasing ΔT, causing the state to contract toward the zero vector (or, equivalently to its initial state). Intuitively, it means that as more time passes (since the last observation), the impact of historical arrivals begin to diminish. In the limit, time-triggered reset mechanism forces the state representation to reset to its initial state. This leads to an interesting alternative interpretation of the exponential basis functions: we are effectively learning a *dynamic forgetting process*, in which the *forget rates* are regulated with the help of exponential basis functions.

Lipschitz Continuity. The mapping $\gamma : \mathbb{R}_+ \to [0, 1]$ is the exponential decay function defined as $\gamma(\Delta T) = \exp\{-\max(0, W\Delta T + b)\}$, where $W > 0$ and $b \in \mathbb{R}$ are fixed scalar parameters. Then, γ is Lipschitz continuous on $\mathbb{R}_+$, with Lipschitz constant:

$$L = W \cdot \exp(-b).$$

Refer to the detailed proof in Appendix 1.1. This result establishes that the exponential basis function $\gamma(\Delta T)$ used in GRUwE is Lipschitz continuous with a closed-form constant that depends directly on the decay weight $\mathbf{W}_\gamma$ and $\mathbf{b}_\gamma$. The decay function is guaranteed not to change faster than $W \cdot \exp(-b)$, enabling GRUwE to dynamically adjust the the smoothness of the exponential decay function and ensuring that the function evolves smoothly over time.

6 Empirical Evaluation

We evaluate the performance of GRUwE on both next observation and next event prediction tasks.

Datasets. For next observation prediction, we use four irregularly sampled multivariate time series datasets: the United States Historical Climatology Network (USHCN), which contains weather-related attributes, and three clinical datasets: PhysioNet, MIMIC-III-Small, and MIMIC-III-Large. Among the four datasets, USHCN is made irregular by randomly masking 50% of the observed time-points as proposed in Schirmer et al. (2022), whereas Physionet, MIMIC-III-Small, and MIMIC-III-Large are irregular in nature. For the event prediction, we use Retweet Zhou et al. (2013) consisting of retweet event sequences; Taxi Whong (2014) consisting of taxi pick-up and drop-off events in five New York city boroughs; Amazon Ni et al. (2019) which consists of sequences of user provided product reviews; StackOverflow Leskovec & Sosič (2016) consisting of sequence of awards received by users on a Q&A website, and Taobao Xue et al. (2022) consisting of user activities on Taobao platform. We provide the description of the datasets in Appendix 2.

Models. For the next observation prediction, we compare the proposed GRUwE models with the SOTA baseline models: GRU-Δ_t Che et al. (2018), RKN-Δ_t Becker et al. (2019), GRU-D Chung et al. (2014), mTAND Shukla & Marlin (2021), CRU Schirmer et al. (2022), f-CRU Schirmer et al. (2022), ODE-RNN Rubanova et al. (2019), Latent ODE Rubanova et al. (2019), ContiFormer Chen et al. (2023), T-PatchGNNZhang et al. (2024), GraFITi Yalavarthi et al. (2024). In the next event prediction task, we compare GRUwE with Recurrent CIF models: RMTPP Du et al. (2016), NHPMei & Eisner (2017); Attention-based CIF approaches including THP Zuo et al. (2020), SAHP Zhang et al. (2020), ATTNHP Yang et al.

Model	USHCN		Physionet		MIMIC-III-Large		MIMIC-III-Small	
	MSE $\times 10^{-2}$	MAE $\times 10^{-2}$	MSE $\times 10^{-2}$	MAE $\times 10^{-2}$	MSE $\times 10^{-2}$	MAE $\times 10^{-2}$	MSE $\times 10^{-1}$	MAE $\times 10^{-1}$
f-CRU	0.020± 0.007	0.455± 0.077	1.095± 0.069	5.295± 0.132	1.191± 0.043	6.535± 0.214	7.808± 0.021	5.963± 0.029
mTAND	0.007± 0.004	0.194± 0.069	0.330± 0.015	3.411± 0.130	1.260± 0.018	6.885± 0.082	5.960± 0.003	5.087± 0.017
GRU-D	0.015± 0.009	0.386± 0.110	0.672± 0.026	5.459± 0.094	0.984± 0.028	5.853± 0.102	6.621± 0.012	5.486± 0.032
Latent ODE	0.007± 0.004	0.127± 0.031	0.676± 0.005	5.302± 0.001	1.209± 0.018	6.490± 0.049	6.658± 0.010	5.547± 0.026
ContiFormer	**0.005** ± 0.002	**0.125** ± 0.016	0.479± 0.024	4.232± 0.001	1.348± 0.093	6.941± 0.399	7.119± 0.022	5.873± 0.035
ODE-RNN	0.019± 0.017	0.220± 0.116	0.770± 0.042	5.519± 0.273	1.429± 0.046	7.251± 0.262	6.401± 0.008	5.302± 0.017
CRU	0.030± 0.019	0.519± 0.166	0.807± 0.035	5.233± 0.242	1.236± 0.035	6.735± 0.139	6.927± 0.018	5.812± 0.030
RKN-Δ_t	0.015± 0.016	0.367± 0.178	0.680± 0.042	4.854± 0.197	1.292± 0.042	6.820± 0.081	8.205± 0.025	6.185± 0.043
GRU-Δ_t	0.035± 0.001	0.717± 0.018	0.449± 0.018	4.160± 0.154	1.414± 0.051	7.226± 0.086	6.863± 0.019	5.617± 0.031
T-PatchGNN	0.065± 0.031	0.909± 0.405	0.338± 0.032	3.259± 0.168	1.226± 0.010	6.689± 0.151	5.664± 0.004	4.777± 0.016
GraFITi	0.074± 0.015	0.673± 0.042	**0.233** ± 0.009	**2.781** ± 0.025	1.419± 0.032	7.448± 0.121	4.692± 0.003	**4.287** ± 0.021
HyperIMTS	0.052± 0.013	0.539± 0.021	0.269± 0.003	2.932± 0.020	OOM	OOM	4.734± 0.008	4.364± 0.015
GRUwE	0.015± 0.013	0.377± 0.187	0.261± 0.006	2.957± 0.035	**0.816** ± 0.026	**5.278** ± 0.036	**4.651** ± 0.015	4.296± 0.022

Table 1: **Next observation prediction.** Comparison of models on next observation prediction on USHCN, Physionet MIMIC-III-Small and MIMIC-III-Large datasets. We report the mean and standard deviation of MSE and MAE on five distinct random seeds. "OOM" refers to out-of-memory GPU error triggered during training.

(2022) and Cumulative CIF approach FullyNN Omi et al. (2019). We include more details on the implementation of the baselines in the Appendix 3).

Model Training. For the next observation prediction task, the models processes a masked multivariate time series input, where the future observation are omitted. Models are optimized to output the entire input sequence after observing partially masked sequence. We use Mean Squared Error (MSE) loss function to optimize the model parameters. Concretely, for a sequence s with N masked time steps, prediction horizon ΔT, observation mask vector $\mathbf{m}_{t+\Delta T}$, prediction values $\hat{\mathbf{x}}_{t,\Delta T}$ and observed values $\mathbf{x}_{t,\Delta T}$, we optimize the model parameters by minimizing the masked MSE loss:

$$\mathcal{L}_{\text{obs}}(s) = \frac{1}{\sum_{i=1}^{N} \mathbf{m}_{t+\Delta T}^{(i)}} \sum_{i=1}^{N} \mathbf{m}_{t+\Delta T}^{(i)} \cdot \left(\hat{\mathbf{x}}_{t,\Delta T}^{(i)} - \mathbf{x}_{t,\Delta T}^{(i)}\right)^2 \tag{10}$$

For the event prediction task, conditional intensity function parameterized with the help of GRUwE is optimized by maximizing the log-likelihood of observing a sequence $s = \{(\tau_j, k_j)\}_{j=1}^{L}$ at observation times $\{\tau_1, \tau_2, ..., \tau_L\} \in [0, T]$:

$$\mathcal{L}_{event}(s) = \sum_{j=1}^{L} log\lambda(t_j|\mathcal{H}_j, k_j) - \int_{t=0}^{T} \lambda(t|\mathcal{H}_t)\, dt. \tag{11}$$

where the total intensity function is given by: $\lambda(t|\mathcal{H}_t) = \sum_{k=1}^{K} \lambda(t|\mathcal{H}_t \mid k)$.

Evaluation Criteria. For the next observation prediction, similar to prior works Schirmer et al. (2022); Yalavarthi et al. (2024); Zhang et al. (2024) we evaluate models on MSE and Mean Absolute Error (MAE) on the masked future values on the sequences in the test split. Using standard evaluation metrics in event prediction literature Yang et al. (2022); Zuo et al. (2020); Zhang et al. (2020), we compare the model quality on the test set using: RMSE: Root Mean Squared Error in predicting the next event arrival time; ER: short for Error Rate, is the percentage of incorrectly predicted next event type and the log-likelihood of the next observed event. To ensure robust evaluation, we conduct experiments using 5 distinct random seeds and report the mean and standard deviation of the performance metrics.

Hyperparameter search. We conduct model-specific hyperparameter tuning by training various model configurations on the training set and evaluating their performance on the validation set. Hyper-parameter ranges for the methods were adjusted to include the optimal hyper-parameter ranges reported by the original authors. For each model, we select the configuration that achieves the lowest validation MSE (for forecasting) and lowest validation LL (for event prediction) and report its test performance. We include more details on the hyperparameter tuning in Appendices 4 to 9.

7 Results and Discussion

We evaluate the proposed GRUwE model on next observation prediction and next event prediction tasks.

Next observation prediction. We evaluate the performance of GRUwE and baselines by predicting the

[1]Original FullyNN model does not support multi-type event.

Model	Taxi		Retweet		StackOverflow		Amazon		Avg.
	RMSE(↓)	ER(↓)	RMSE(↓)	ER(↓)	RMSE(↓)	ER(↓)	RMSE(↓)	ER(↓)	Rank (↓)
FullyNN [1]	0.373± 0.005	N.A.	**21.92** ±0.159	N.A.	1.375±0.015	N.A.	0.615±0.005	N.A.	4.75
NHP	**0.369** ± 0.001	9.22±0.005	22.32± 0.001	**40.25** ± 0.002	1.369±0.001	55.78±0.007	0.612±0.001	68.30±0.009	2.88
A-NHP	0.370± 0.000	11.42±0.016	22.28±0.018	41.05±0.004	1.370±0.000	55.51±0.001	0.612±0.000	**65.65** ±0.002	3.38
THP	**0.369** ± 0.000	8.85± 0.003	22.32±0.001	**40.25** ±0.002	**1.368** ±0.002	55.60±0.003	0.612±0.000	66.72±0.009	2.13
SAHP	0.372±0.003	9.75± 0.001	22.40±0.301	41.60±0.002	1.375±0.013	56.10±0.005	0.619±0.005	67.70±0.006	5.38
RMTPP	0.370±0.000	9.86±0.009	22.31±0.209	44.10±0.003	1.370±0.001	57.50±0.000	0.634±0.011	73.66±0.052	5.25
GRUwE	**0.369** ±0.000	**8.58** ±0.003	22.21±0.134	40.81±0.004	1.369±0.001	**55.34** ±0.004	**0.611** ±0.001	67.24±0.004	**1.75**

Table 2: **Next event prediction.** Model performance comparison for the next event prediction on the Taxi, Retweet, StackOverflow and Amazon datasets. We report the mean and standard deviation of the metrics on five distinct random seeds. For RMSE and ER metrics, lower is better.

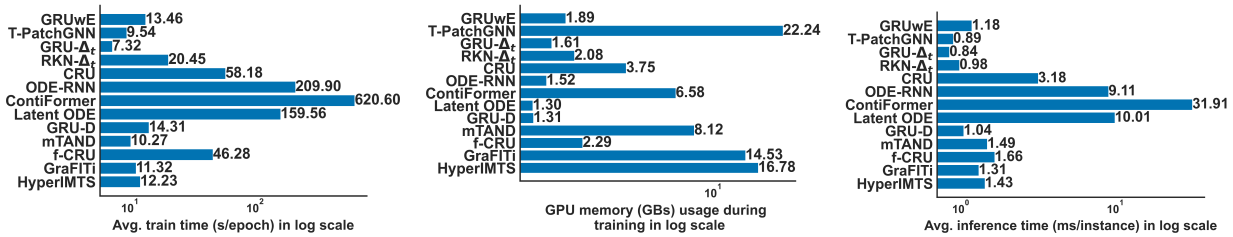

(a) (b) (c)

Figure 2: **Computational cost analysis on retrospective data.** (**2a**) compares the train times for all models; (**2b**) compares the peak GPU memory usage during training; **(2c)** compares the inference times on retrospective data. Lower is better for all plots.

next observation for each variable defining the multivariate time series given the history of past observations. For the Physionet dataset, the model observes the first 24 hours of the total 48-hour period to predict the next observations for all (37) variables. Similarly, for the USHCN dataset, with daily samples over four years, we use the first half to predict the next observation for all 5 variables. For the MIMIC-III-Large dataset, models consider values of 506 variables over past 48 hours from a randomly sampled time point in the patient record. The models are compared on predicted values for the next observations made on 363 numerical variables representing vital signs and labs. For the MIMIC-III-Small dataset, the model observes the first half of the 96 numerical variables to predict their next observation. Table 1 presents the predictive performance of all models on the next observation prediction task across the four datasets, evaluated over multiple random seeds. Next we briefly summarize the results on individual datasets below. On the USHCN dataset, ContiFormer, Latent ODE, mTAND are the top performing models in terms of MSE and MAE. On the Physionet dataset, GraFITi, GRUwE and HyperIMTS are the top performing methods. On the MIMIC-III-Large dataset, GRUwE achieves the lowest MSE and MAE, outperforming all competing models, with GRU-D ranking second among the baselines. GRU-D uses a mean-reverting interpolation scheme for missing inputs, an assumption that likely holds for this setting, which we believe is contributing to its competitive predictive accuracy. We note that MIMIC-III-Large is the most challenging dataset of all the datasets used: it consists of high-dimensional input observations and highly varied observation sequence lengths as reported in Table 4. On the MIMIC-III-Small dataset, GRUwE outperforms all the baseline models. GraFITi and HyperIMTS remain competitive.

Missing data perspective. Prior works Singh (1997); Ramoni & Sebastiani (1997) have classified the observed missingness in the data into three categories: i) Missing Completely at Random (MCAR), and ii) Missing at Random, and iii) Not Missing at Random (NMAR). In our experiments, USHCN belongs to MCAR, where the missingness is synthetically introduced by dropping the observations uniformly at random. In contrast, the Physionet and MIMIC-III datasets are instances of NMAR, where missingness is contextual, i.e., *dependent* on observed and unobserved values. For example, in these datasets, a laboratory test might be missing until an abnormal vital sign value is observed, making the physician order the test. Our analysis on next observation prediction suggests that while GRUwE remain moderately competitive in MCAR, it is more competitive, and in fact, outperforms all the models in 2 out of 3 datasets on NMAR. These results demonstrates that GRUwE is better able to model the dependencies inherent in the processes generating the missingness.

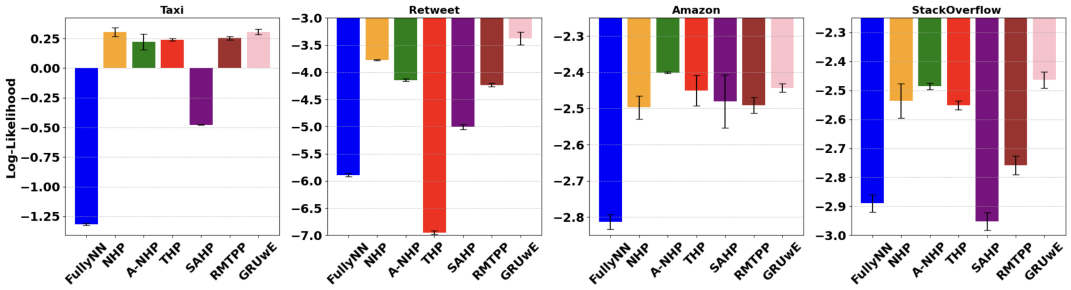

Figure 3: Comparison of Log-Likelihood (LL) for all the TPP models on next event prediction task. A higher value of LL indicates a better fit.

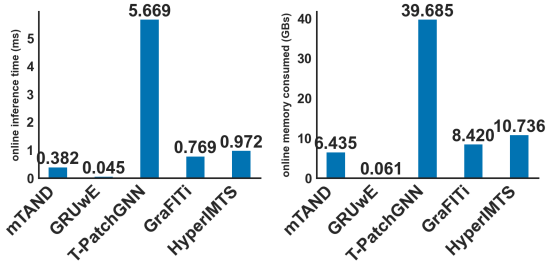

(a)

Step	Code
Time decay	`gamma = exp(-relu(W@T))`
Decay state	`g_t = gamma * h_prev`
Concat input	`x_mask = [x, mask]`
GRU update	`h_t = GRU(x_mask, g_t)`

(b)

Figure 4: (**a**) Comparison of inference time (**left**) and memory consumption (**right**) in online deployment. Lower is better in both cases. (**b**) GRUwE's step function pseudocode.

Next event prediction. We report the comparison of the TPP models in the Table 2 and plot the log-likelihoods in Figure 3. Notably, the FullyNN model Omi et al. (2019) is designed for single event prediction. While RMSE and LL metrics can be computed, the ER metric cannot be evaluated for this model in our comparison. As demonstrated in Figure 3, GRUwE outperforms all intensity-based models in terms of log-likelihood comparison, except on the Amazon dataset, where it achieves the second-highest performance. For the Taxi dataset, which has the least number of training sequences across all datasets, GRUwE ranks first in terms of the RMSE and ER. If we compare among all RNN-based intensity models (i.e. GRUwE, NHP, RMTPP), GRUwE demonstrates the best performance on all metrics and datasets showing the effectiveness of the proposed approach.

Rank analysis. Overall, our results in the Table 2 indicate that GRUwE is consistently among the top performing models across all the datasets and evaluation metrics. To assess its benefits more rigorously, we summarize the results by adding a new rank-based metric that calculates the average rank of each model across all datasets for both RMSE and ER metrics. The ranking results show that GRUwE achieves the highest rank score of **1.75**, while the second-best THP model has the score 2.13. More details on this rank analysis is provided in the Appendix 10.

Differences to GRU-D Che et al. (2018). GRUwE is most closely related to the perviously proposed GRU-D model since it also combines GRU and exponential decay functions. However, the following key differences remain. While GRU-D imputes the input missing values by learning exponential schedules to revert to its empirical mean, GRUwE lifts this mean-reverting assumption by applying zero imputation to deal with missingness. This reduces the cascading error in the final prediction due to errors in imputation. GRU-D was proposed for the classification tasks, and it is unclear how it can be adapted to perform continuous-time predictions. GRUwE addresses this by introducing the flexible prediction module. GRUwE simplifies GRU-D's Markov state representation significantly by removing the need to store and update: i) last observed variable values, ii) their respective time elapsed since observation, and iii) empirical mean for each variable. It is important to highlight that all of these differences make GRUwE a simpler model compared to GRU-D while significantly boosting the predictive accuracy.

Computational cost analysis. In addition to comparison of predictive performance of the models, we also analyze their computational costs, in particular their training time, inference time and peak memory

Model	USHCN (MSE $\times 10^{-2}$)	Physionet (MSE $\times 10^{-2}$)	MIMIC-III-Large (MSE $\times 10^{-2}$)	MIMIC-III-Small (MSE $\times 10^{-1}$)
GRU-Lin	0.019	0.925	1.532	7.573
GRU-Sin	0.016	0.359	1.216	7.324
GRUwE-DualExp	**0.013**	0.269	0.854	4.670
GRUwE-FrozenExp	0.016	<u>0.256</u>	<u>0.848</u>	<u>4.665</u>
GRUwE	<u>0.014</u>	**0.253**	**0.831**	**4.650**

Table 3: **GRUwE ablation comparison**. GRUwE variants modify the time basis function: using linear or sinusoidal functions, learning separate basis for transition and prediction, and freezing the randomly initialized exponential basis.

consumption. The results are summarized in Figures 2 and 4a and a more detailed discussion on computational efficiency is included in the Appendix 11. In terms of training time on retrospective data, as shown in Figure 2a, models that can be parallelized over the time dimension (T-PatchGNN, mTAND, GraFITi, HyperIMTS) are the fastest, RNN methods (GRUwE, GRU-D, GRU-Δ_t) rank second, models with linear dynamics (RKN-Δ_t, CRU, f-CRU) rank third and lastly, models that require invoking numerical solvers (ContiFormer, Latent ODE, ODE-RNN) consume the most amount of train time. The computational performance trade-off is clear from Figure 2b: models that can be parallelized in time dimension offer the best training times at the expense of significantly higher memory consumption. After training the models on retrospective data, we evaluate their inference time in two settings: (i) **retrospective inference** in Figure 2c, where the model processes the entire history at once to predict the next observation, and (ii) **online inference**, which simulates real-world deployment by sequentially receiving streamed observations, updating its state, and making predictions for future times in real-time. For the online inference especially, since the process generating the data is sequential in nature, having a compact Markov state representation and efficient state update mechanism require much less computational resources than models that need to buffer all the historical observations and re-process them every time a new observation arrives. Moreover, this buffer grows over time which increases memory consumption and inference time thus, creating a computational bottleneck. Figure 4a demonstrates that GRUwE, with its compact Markov state representation, incurs significantly lower computational overhead in online inference setting compared to the baseline methods that offer the fastest training times and rank among the top performers in the next observation prediction task.
Easy to implement. As shown in Figure 4b, GRUwE's reset state mechanisms can be implemented in just a few lines of code as it builds on the components that are natively supported by most modeling packages. An easy model implementation is preferred not only because it improves readability, but also reduces the scope for introducing bugs, making the model easier to port, reproduce, debug, and maintain.
GRUwE ablation analysis. To better assess the contribution of the proposed GRUwE model, we conduct a series of architectural ablation studies. Specifically, we investigate: (i) how GRUwE compares to variants that employ alternative time basis functions, such as learnable linear (GRU-Lin) or sinusoidal (GRU-Sin) basis; (ii) how the predictive performance changes when model complexity is increased by using *separate* learnable exponential function for the transition and prediction functions (GRUwE-DualExp); and (iii) how performance is affected when model complexity is reduced by *freezing* the randomly initialized exponential basis (GRUwE-FrozenExp) during model training. Across all datasets (as presented in Table 3), GRUwE consistently matches or outperforms its ablated variants, highlighting the importance of a shared, learnable exponential basis. Replacing the exponential basis with linear or sinusoidal functions degrades performance significantly. This supports our hypothesis that exponentials provide a better inductive bias, as their memoryless, multiplicative form makes temporal effects naturally composable over arbitrary time gaps. Learning separate exponential basis for the transition and prediction functions helps in one but does not outperform GRUwE in most cases, suggesting that sharing a single temporal basis regularizes the training and yields a more robust temporal representation. Lastly, reducing the complexity by freezing the exponential basis yields competitive but worse performance in all cases, indicating that adapting decay rates to the task is important.

Limitations. Unlike compared baselines such as mTAND and CRU, our proposed architecture, GRUwE doesn't have a built-in notion of uncertainty, and we consider incorporating it in the future work will be an

exciting extension of our current work.

8 Conclusion

In summary, this work revisits the challenge of modeling irregularly sampled multivariate time series through the lens of simplicity and computational efficiency. By introducing GRUwE, we demonstrate that a principled extension of the GRU architecture, augmented with learnable exponential basis functions, can achieve SOTA predictive performance across both continuous-time forecasting and event prediction tasks, while remaining significantly computationally efficient during inference in the online deployment. These results demonstrate that carefully designed recurrent architectures grounded in classical principles, can compete or outperform more complex neural and differential-equation–based models. We believe these findings offer clear guidance for future research on irregular time series modeling.

References

Philipp Becker, Harit Pandya, Gregor Gebhardt, Cheng Zhao, C. James Taylor, and Gerhard Neumann. Recurrent kalman networks: Factorized inference in high-dimensional deep feature spaces. In Kamalika Chaudhuri and Ruslan Salakhutdinov (eds.), *Proceedings of the 36th International Conference on Machine Learning*, volume 97 of *Proceedings of Machine Learning Research*, pp. 544–552. PMLR, 09–15 Jun 2019. URL https://proceedings.mlr.press/v97/becker19a.html.

Zhengping Che, Sanjay Purushotham, Kyunghyun Cho, David Sontag, and Yan Liu. Recurrent neural networks for multivariate time series with missing values. *Scientific Reports*, 8(1), April 2018. ISSN 2045-2322. doi: 10.1038/s41598-018-24271-9. URL http://dx.doi.org/10.1038/s41598-018-24271-9.

Ricky TQ Chen, Yulia Rubanova, Jesse Bettencourt, and David K Duvenaud. Neural ordinary differential equations. *Advances in neural information processing systems*, 31, 2018.

Ricky TQ Chen, Brandon Amos, and Maximilian Nickel. Neural spatio-temporal point processes. In *International Conference on Learning Representations*, 2020.

Yuqi Chen, Kan Ren, Yansen Wang, Yuchen Fang, Weiwei Sun, and Dongsheng Li. Contiformer: Continuous-time transformer for irregular time series modeling. In *Thirty-seventh Conference on Neural Information Processing Systems*, 2023.

Junyoung Chung, Caglar Gulcehre, KyungHyun Cho, and Yoshua Bengio. Empirical evaluation of gated recurrent neural networks on sequence modeling, 2014. URL https://arxiv.org/abs/1412.3555.

Edward De Brouwer, Jaak Simm, Adam Arany, and Yves Moreau. Gru-ode-bayes: Continuous modeling of sporadically-observed time series. In H. Wallach, H. Larochelle, A. Beygelzimer, F. d'Alché-Buc, E. Fox, and R. Garnett (eds.), *Advances in Neural Information Processing Systems*, volume 32. Curran Associates, Inc., 2019. URL https://proceedings.neurips.cc/paper_files/paper/2019/file/455cb2657aaa59e32fad80cb0b65b9dc-Paper.pdf.

Nan Du, Hanjun Dai, Rakshit Trivedi, Utkarsh Upadhyay, Manuel Gomez-Rodriguez, and Le Song. Recurrent marked temporal point processes: Embedding event history to vector. In *Proceedings of the 22nd ACM SIGKDD international conference on knowledge discovery and data mining*, pp. 1555–1564, 2016.

Albert Gu and Tri Dao. Mamba: Linear-time sequence modeling with selective state spaces. *arXiv preprint arXiv:2312.00752*, 2023.

Sepp Hochreiter and Jürgen Schmidhuber. Long short-term memory. *Neural Computation*, 9(8):1735–1780, November 1997. ISSN 1530-888X. doi: 10.1162/neco.1997.9.8.1735. URL http://dx.doi.org/10.1162/neco.1997.9.8.1735.

Alistair Johnson, Tom Pollard, and Roger Mark. Mimic-iii clinical database, 2023. URL https://physionet.org/content/mimiciii/.

Rudolf Emil Kalman. Mathematical description of linear dynamical systems. *Journal of the Society for Industrial and Applied Mathematics, Series A: Control*, 1(2):152–192, 1963.

Patrick Kidger, James Morrill, James Foster, and Terry Lyons. Neural controlled differential equations for irregular time series. *Advances in Neural Information Processing Systems*, 33:6696–6707, 2020.

Diederik Kingma and Jimmy Ba. Adam: A method for stochastic optimization. In *International Conference on Learning Representations (ICLR)*, San Diega, CA, USA, 2015.

Jure Leskovec and Rok Sosič. Snap: A general-purpose network analysis and graph-mining library. *ACM Transactions on Intelligent Systems and Technology (TIST)*, 8(1):1–20, 2016.

Boyuan Li, Yicheng Luo, Zhen Liu, Junhao Zheng, Jianming Lv, and Qianli Ma. Hyperimts: Hypergraph neural network for irregular multivariate time series forecasting. *arXiv preprint arXiv:2505.17431*, 2025.

Yicheng Luo, Bowen Zhang, Zhen Liu, and Qianli Ma. Hi-patch: Hierarchical patch gnn for irregular multivariate time series. In *Forty-second International Conference on Machine Learning*, 2025.

Ivan Marisca, Andrea Cini, and Cesare Alippi. Learning to reconstruct missing data from spatiotemporal graphs with sparse observations. *Advances in Neural Information Processing Systems*, 35:32069–32082, 2022.

Hongyuan Mei and Jason M Eisner. The neural hawkes process: A neurally self-modulating multivariate point process. *Advances in neural information processing systems*, 30, 2017.

MJ Menne, CN Williams Jr, and RS Vose. Long-term daily and monthly climate records from stations across the contiguous united states (us historical climatology network). Technical report, Environmental System Science Data Infrastructure for a Virtual Ecosystem ..., 2016.

Jianmo Ni, Jiacheng Li, and Julian McAuley. Justifying recommendations using distantly-labeled reviews and fine-grained aspects. In *Proceedings of the 2019 conference on empirical methods in natural language processing and the 9th international joint conference on natural language processing (EMNLP-IJCNLP)*, pp. 188–197, 2019.

Takahiro Omi, Kazuyuki Aihara, et al. Fully neural network based model for general temporal point processes. *Advances in neural information processing systems*, 32, 2019.

Marco Ramoni and Paola Sebastiani. Robust parameter learning in bayesian networks with missing data. In *Sixth International Workshop on Artificial Intelligence and Statistics*, pp. 399–406. PMLR, 1997.

Yulia Rubanova, Ricky T. Q. Chen, and David K Duvenaud. Latent ordinary differential equations for irregularly-sampled time series. In H. Wallach, H. Larochelle, A. Beygelzimer, F. d'Alché-Buc, E. Fox, and R. Garnett (eds.), *Advances in Neural Information Processing Systems*, volume 32. Curran Associates, Inc., 2019. URL https://proceedings.neurips.cc/paper_files/paper/2019/file/42a6845a557bef704ad8ac9cb4461d43-Paper.pdf.

Mona Schirmer, Mazin Eltayeb, Stefan Lessmann, and Maja Rudolph. Modeling irregular time series with continuous recurrent units. In Kamalika Chaudhuri, Stefanie Jegelka, Le Song, Csaba Szepesvari, Gang Niu, and Sivan Sabato (eds.), *Proceedings of the 39th International Conference on Machine Learning*, volume 162 of *Proceedings of Machine Learning Research*, pp. 19388–19405. PMLR, 17–23 Jul 2022. URL https://proceedings.mlr.press/v162/schirmer22a.html.

Satya Narayan Shukla and Benjamin Marlin. Multi-time attention networks for irregularly sampled time series. In *International Conference on Learning Representations*, 2021. URL https://openreview.net/forum?id=4c0J6lwQ4_.

Robert H. Shumway and David S. Stoffer. *Time Series Analysis and Its Applications (4th edition)*. Springer-Verlag, Berlin, Heidelberg, 2017.

Sima Siami-Namini, Neda Tavakoli, and Akbar Siami Namin. A comparison of arima and lstm in forecasting time series. In *2018 17th IEEE International Conference on Machine Learning and Applications (ICMLA)*, pp. 1394–1401, 2018. doi: 10.1109/ICMLA.2018.00227.

Ikaro Silva, George Moody, Daniel J Scott, Leo A Celi, and Roger G Mark. Predicting in-hospital mortality of icu patients: The physionet/computing in cardiology challenge 2012. In *2012 Computing in Cardiology*, pp. 245–248. IEEE, 2012.

Moninder Singh. Learning bayesian networks from incomplete data. *AAAI/IAAI*, 1001:534–539, 1997.

Jimmy TH Smith, Andrew Warrington, and Scott W Linderman. Simplified state space layers for sequence modeling. In *ICLR*, 2023.

Yusuke Tashiro, Jiaming Song, Yang Song, and Stefano Ermon. Csdi: Conditional score-based diffusion models for probabilistic time series imputation. *Advances in Neural Information Processing Systems*, 34: 24804–24816, 2021.

Chris Whong. Foiling nyc's taxi trip data. *FOILing NYCs Taxi Trip Data. Np*, 18:14, 2014.

Siqiao Xue, Xiaoming Shi, James Zhang, and Hongyuan Mei. Hypro: A hybridly normalized probabilistic model for long-horizon prediction of event sequences. *Advances in Neural Information Processing Systems*, 35:34641–34650, 2022.

Vijaya Krishna Yalavarthi, Kiran Madhusudhanan, Randolf Scholz, Nourhan Ahmed, Johannes Burchert, Shayan Jawed, Stefan Born, and Lars Schmidt-Thieme. Grafiti: Graphs for forecasting irregularly sampled time series. In *Proceedings of the AAAI Conference on Artificial Intelligence*, volume 38, pp. 16255–16263, 2024.

Chenghao Yang, Hongyuan Mei, and Jason Eisner. Transformer embeddings of irregularly spaced events and their participants. In *Proceedings of the tenth international conference on learning representations (ICLR)*, 2022.

Qiang Zhang, Aldo Lipani, Omer Kirnap, and Emine Yilmaz. Self-attentive hawkes process. In *International conference on machine learning*, pp. 11183–11193. PMLR, 2020.

Weijia Zhang, Chenlong Yin, Hao Liu, Xiaofang Zhou, and Hui Xiong. Irregular multivariate time series forecasting: A transformable patching graph neural networks approach. In *Forty-first International Conference on Machine Learning*, 2024.

Xiang Zhang, Marko Zeman, Theodoros Tsiligkaridis, and Marinka Zitnik. Graph-guided network for irregularly sampled multivariate time series. In *International Conference on Learning Representations, ICLR*, 2022.

Ke Zhou, Hongyuan Zha, and Le Song. Learning triggering kernels for multi-dimensional hawkes processes. In *International conference on machine learning*, pp. 1301–1309. PMLR, 2013.

Simiao Zuo, Haoming Jiang, Zichong Li, Tuo Zhao, and Hongyuan Zha. Transformer hawkes process. In *International conference on machine learning*, pp. 11692–11702. PMLR, 2020.

Appendix

Table of Contents

1 Theory

1.1 Lipschitz Continuity of Exponential Decay Function

Theorem 1.1 (**Lipschitz Continuity of Exponential Decay Function**). *Let $\gamma : \mathbb{R}_+ \to \mathbb{R}$ be the exponential decay function defined as*

$$\gamma(\Delta T) = \exp\left\{-\max\left(0, W\Delta T + b\right)\right\},$$

where $W > 0$ and $b \in \mathbb{R}$ are fixed scalar parameters. Then, γ is Lipschitz continuous on $\mathbb{R}_+$, with Lipschitz constant

$$L = W \cdot \exp(-b).$$

Proof. We first compute the derivative of γ with respect to ΔT in piecewise form:

$$\frac{d}{d\Delta T}\gamma(\Delta T) = \begin{cases} 0, & \text{if } \Delta T \leq -\frac{b}{W}, \\ -W \cdot \exp\left(-W\Delta T - b\right), & \text{if } \Delta T > -\frac{b}{W}. \end{cases}$$

Observe that γ is continuous everywhere and differentiable almost everywhere (it is non-differentiable only at the point $\Delta T = -\frac{b}{W}$). The function γ is Lipschitz continuous if its derivative is bounded almost everywhere, and the essential supremum of the absolute value of the derivative gives the Lipschitz constant.

For $W\Delta T + b > 0$, the magnitude of the derivative is:

$$\left|\frac{d\gamma}{d\Delta T}\right| = W \cdot \exp(-W\Delta T - b).$$

The maximum of this expression over $\Delta T \in \mathbb{R}_+$ occurs at $\Delta T = 0$, giving:

$$\left|\frac{d\gamma}{d\Delta T}\right| \leq W \cdot \exp(-b).$$

For $\Delta T < -\frac{b}{W}$, the derivative is zero. Therefore, the global Lipschitz constant is:

$$L = \sup_{\Delta T \geq 0} \left|\frac{d\gamma}{d\Delta T}\right| = W \cdot \exp(-b).$$

□

1.2 Monotonic Latent Dynamics

Remark 1 (**Exponential Basis Functions Induces Growth and Decay**). *Exponential basis functions can induce exponentially growing and decaying trends in the state as a function of time elapsed.*

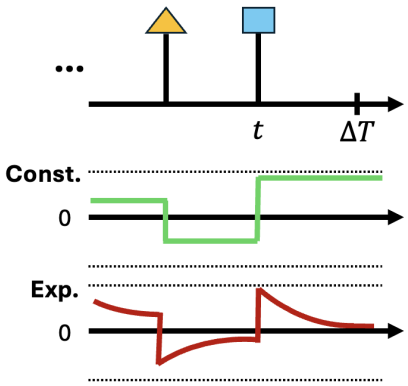

Figure 5: An abstract diagram of latent dynamics in the case of GRU (**top**) and GRUwE (**bottom**) highlighting that GRUwE can recover monotonic latent dynamics between two consecutive event or observation arrivals.

We note that $\boldsymbol{\gamma(\Delta T)} \in (0, 1]^D$, the i^{th} component of state is bounded, i.e., $h_{t,i} \in [-1, 1]$. Since $\mathbf{g}_{t,\Delta T} = \boldsymbol{\gamma(\Delta T)} \odot \mathbf{h}_t$, if $h_{t,i} \in [-1, 0)$, then $h_{t+\Delta T,i} \geq h_{t,i}$. Basically, the transformed state value is an upper-bound of the initial value if it is negative. If the initial value is positive, then the transformed value is a lower-bound: i.e., $h_{t,i} \in (0, 1]$, then $h_{t+\Delta T,i} \leq h_{t,i}$. Therefore, depending on the state $\mathbf{h}_t$, the exponential basis function update can cause the state value to grow or decay exponentially. This property makes exponential basis functions highly expressive for time-series modeling.

2 Datasets

2.1 USHCN

United States Historical Climatology Network (USHCN) Menne et al. (2016) is a publicly available dataset (`https://data.ess-dive.lbl.gov/view/doi%3A10.3334%2FCDIAC%2FCLI.NDP019`) consisting of daily measurements of 5 meteorological variables including min temperature, max temperature, precipitation, snowfall, and snow depth from 1218 observing stations across the United States. It is worth noting that there are multiple versions of datasets extracted from USHCN that have been used to evaluate irregularly sampled tim series. We extract the dataset in our analysis using the steps mentioned in Schirmer et al. (2022). We mimic their data pre-processing pipeline by: i) sub-selecting 1168 stations over a 4-year period ranging from 1990 to 1993 ii) subsample 50% of time-points to increase irregularities in time dimension; and setting unobserved rate to 20% to increase sparsity of observations, iii) 20% of the entire dataset is used for testing; we train and validate on the remaining 80% data; 25% of that is used for validation.

To be able to compare to methods listed in the Schirmer et al. (2022) for the prediction task, we replicate their: (1) pre-processing logic; (2) splitting of dataset into train, validation and test sets by using the same seed; (3) 20% partial observability in feature dimension and 50% in time dimension in GRUwE run; (4) masking logic for prediction task.

2.2 Physionet

Predicting Mortality of ICU Patients: The PhysioNet/Computing in Cardiology Challenge 2012 Silva et al. (2012) made publicly available (`https://physionet.org/files/challenge-2012/1.0.0/`) 8000 ICU patient stays that span 48 hours reporting 37 clinical real-valued time series variables observed at irregular time-intervals. The dataset includes various variables, including Non-Invasive Mean Arterial Pressure, Platelets, Sodium, and several others. We follow the pre-processing of this dataset described by Schirmer et al. (2022). Observations in time are rounded by 6 minutes. Similar to USHCN, test split consists of 20% of the data, the rest is used for training and validation; validation set consists of 25% of this split.

For fair comparison to methods listed in Schirmer et al. (2022), we ensure (1) 6-minute quantization (as done in Rubanova et al. (2019); Schirmer et al. (2022)); (2) splits are created using the same seeds; (3) same masking logic is applied for prediction task.

2.3 MIMIC-III-Large

In the following, we outline the steps to extract MIMIC-III-Large dataset from the MIMIC-III Johnson et al. (2023) (`https://physionet.org/content/mimiciii/1.4/`). A population cohort of 10,265 hospital admissions (on 8,799 patients) are extracted from MIMIC-III based on the following criteria: i) patient record is recorded in MetaVision critical care information system, ii) the length of the patient record is between 2 and 20 days, iii) the age of the patient is between 18 and 90. From all EHR tables available in MIMIC-III, we extract (irregularly sampled) time series that include vital signs (such as Heart Rate and Mean Arterial Pressure), lab results (such as Glucose and Hemoglobin), administered medications (such as Propofol and Norepinephrine), and procedures (such as Intubation). The vital signs and lab results are numerical time series, while the rest are indicator time series, indicating if and when the event occurred.

We filter out any univariate time series that occurs less than 500 times across all patients in the cohort resulting in total of 506 time series: 393 numerical (vitals and labs), 77 medications and 36 procedures event time series. We define an *A-point*, abbreviated for Anchor-point, as a temporal moment at which a decision-making system can formulate a prediction based on the past sequence of events. We extract A-points from the filtered patient records regularly with frequency of 24 hours i.e. one sample is extracted every 24 hours from the patient record. We standardize all real-valued univariate time series (i.e. vital signs and labs) data using min-max scaling; and encode all other indicator time series as binary value 0/1. Value is 1 if event occurs; 0 otherwise. 80% of the patient hospital admission are used for training and validation (20% of train split); the rest is used for testing. Splits are constructed on disjoint patients.

Additional pre-processing is required to remove missing values encoded as 9999999 in the numerical time series. To remove outliers from univariate time series (for example, very large values of the order of $1e5$),

we filter out observations that fall either in < 0.1 or > 99.9 percentile ranges. Subsampling of A-points is performed as follows:

1. For each split:
    a. For each patient admission record, filter out A-points with less than 50 events in history and prediction window.
    b. Next, randomly sample one A-point from the filtered A-points i.e. one sample per patient admission record.
2. Subsample 1000 A-points from train, 250 from validation and 200 from test set to be used for experimentation.

2.4 MIMIC-III-Small

We adopt the data extraction methodology described in De Brouwer et al. (2019) to derive the MIMIC-III-Small dataset from MIMIC-III Johnson et al. (2023). Each sample comprises 96 time series variables, irregularly observed over a 48-hour long patient visit. For a comprehensive overview of the dataset pre-processing and extraction steps, we refer readers to Appendix K in De Brouwer et al. (2019).

2.5 Dataset Attributes

Table 4 summarizes the mean, standard deviation, minimum and maximum of all the sequences per dataset. Importantly, the MIMIC-III dataset does not undergo any time discretization, resulting in sequence lengths spanning from 105 to 4299. In terms of average length, the order is as follows: USHCN > MIMIC-III-Large > Physionet > MIMIC-III-Small.

Table 4: Sequence length statistics and number of target variables across datasets

Dataset	Sequence length statistics			# Target Variables
	Mean ± S.D.	Min	Max	
USHCN	730.0 ± 0.00	730	730	5
Physionet	72.16 ± 20.93	1	185	37
MIMIC-III-Small	48.15 ± 69.92	2	614	96
MIMIC-III-Large	244.30 ± 288.85	105	4299	393

2.6 Event Prediction Datasets

We provide descriptions of the four real-world publicly available datasets used in the next even prediction benchmark of the paper. We summarize the properties of these datasets after providing the descriptions:

- **Amazon:** This dataset includes time-stamped user product reviews behavior from January, 2008 to October, 2018. Each user has a sequence of produce review events with each event containing the timestamp and category of the reviewed product, with each category corresponding to an event type. We work on a subset of 5200 most active users with an average sequence length of 70 and then end up with K = 16 event types
- **Retweet:** This dataset contains time-stamped user retweet event sequences. The events are categorized into K = 3 types: retweets by "small," "medium" and "large" users. Small users have fewer than 120 followers, medium users have fewer than 1363, and the rest are large users. We work on a subset of 5200 most active users with an average sequence length of 70.
- **Taxi:** This dataset tracks the time-stamped taxi pick-up and drop-off events across the five boroughs of the New York City; each (borough, pick-up or drop-off) combination defines an event type, so there are K = 10 event types in total. We work on a randomly sampled subset of 2000 drivers and each driver has a sequence. We randomly sampled disjoint train, dev and test sets with 1400, 200 and 400 sequences.

- **StackOverflow:** This dataset has two years of user awards on a question-answering website: each user received a sequence of badges and there are K = 22 different kinds of badges in total. We randomly sampled disjoint train, dev and test sets with 1400, 400 and 400 sequences from the dataset.

Table 5 provides a description of number of unique event types (K), the number of events and sequence length statistics across all four datasets used in our experimental evaluation.

Table 5: Statistics of the used datasets for evaluation

Dataset	K	# of Event Tokens			Sequence Length		
		Train	Dev	Test	Min	Mean	Max
Retweet	3	369000	62000	61000	10	41	97
Amazon	16	288000	12000	30000	14	44	94
Taxi	10	51000	7000	14000	36	37	38
StackOverflow	22	90000	25000	26000	41	65	101

3 Baselines

3.1 Baselines for Next Observation Prediction Task

We include the following baseline methods to compare against our proposed model GRUwE on the next observation prediction task.

GRU-Δ_t: We consider recurrent models GRU-Δ_t as our baselines in the comparison. Gated Recurrent Unit Chung et al. (2014) have been proposed to model sequences using a set of parametric update equations. Since GRU is not time-aware, a variant of GRU that also feeds in time elapsed (since the last time-step) along with the input GRU-Δ_t is used in the comparison.

RKN-Δ_t: Recurrent Kalman Networks (RKN) Becker et al. (2019) have been proposed to incorporate uncertainty in time series modeling. Similar to GRU-Δ_t, we include the baseline RKN-Δ_t that includes time elapsed as an additional input to the model.

GRU-D: We compare our method to Gated Recurrent Unit-Decay (GRU-D) Che et al. (2018) that uses a mean-reverting imputation function for missing variables; applies learnable exponential decays in the input and latent dimension to account for irregular observed times.

mTAND: We evaluate our performance against the Encoder-Decoder generative model, Multi-Time Attention Network (mTAND-Full) Shukla & Marlin (2021), which defines reference points and represents continuous time-points with learnable embeddings to encode their relationship and generate predictions.

CRU and f-CRU: We consider Continuous Recurrent Units (CRU) and fast-Continuous Recurrent Units (f-CRU) Schirmer et al. (2022) as our baselines for prediction tasks. f-CRU is a fast implementation of jointly proposed CRU method. CRU consists of an encoder-decoder framework where the hidden state progression is governed by linear stochastic differential equation that allow incorporating arbitrary time-intervals between observations.

ODE-RNN and Latent ODE: In our analysis, we consider Latent ODE and ODE-RNN proposed in Rubanova et al. (2019) as comparative baselines. ODE-RNN model consist of latent states that adhere to ODE between observations and are updated at observations using standard RNN update equations. Latent ODE model adopts variational auto-encoder framework wherein the hidden state posterior is modeled by an ODE-RNN model. We used the configuration of Latent ODE with ODE-RNN encoder.

ContiFormer: We incorporate ContiFormer Chen et al. (2023) as one of our baselines for the prediction tasks. It builds upon the original transformer architecture by first extending the input irregular data to the continuous-time latent representation by assuming that the underlying dynamics are governed by the ODEs.

T-PatchGNN: We include T-PatchGNN Zhang et al. (2024) as one of our baselines for the prediction tasks. T-PatchGNN first segments each time series into patches of uniform temporal resolution followed by the transformer and time-adaptive GNNs to capture dependencies in the multivariate time series. We use the official T-PatchGNN code made publicly available here: `https://github.com/usail-hkust/t-PatchGNN` in our experiment pipeline.

GraFITi: We add GraFITi Yalavarthi et al. (2024) as one of our baselines for comparisons on the next observation prediction task. GraFITi casts the time series prediction task in terms of edge weight prediction problem after converting the time series to a sparse graph structure. To incorporate this method, we make use of the official implementation available here: `https://github.com/yalavarthivk/GraFITi`.

HyperIMTS: We include HyperIMTS Li et al. (2025) as one of baselines for the next observation prediction task. HyperIMTS models the irregular time series by constructing a hypergraph from observations and learning dependencies with the help of hyperedges connecting the observation nodes. We use the official implementation made available by the authors from this site: `https://github.com/Ladbaby/PyOmniTS`.

3.2 Baselines for Event Prediction Task

We include the following temporal point process baselines for event prediction benchmark.
FullyNN: We add Fully Neural Network (FullyNN) Omi et al. (2019) to our comparison on the next event prediction task. FullyNN learns a cumulative hazard function for modeling the point process intensities. We use the publicly available implementation of this method from here: `https://github.com/ant-research/EasyTemporalPointProcess`
NHP: We include Neural Hawkes Process (NHP) Mei & Eisner (2017) as one of our baselines for the next event prediction task. NHP develops a continuous-time intensity model using the LSTM architecture. We use the publicly available implementation of this method from here: `https://github.com/ant-research/EasyTemporalPointProcess`
A-NHP: We include Attention-Neural Hawkes Process (A-NHP) Yang et al. (2022) as a baseline model for next event prediction task. A-NHP with the help of attention mechanism further refines the NHP architecture to define novel intensity functions. Official code for this method is publicly available at `https://github.com/yangalan123/anhp-andtt`. We used the adapted versions from: `https://github.com/ant-research/EasyTemporalPointProcess`.
THP: Transformer Hakwes Process (THP) Zuo et al. (2020) is included in the comparison for next event prediction task. THP defines the intensity function using the transformer architecture. We use the publicly available implementation of this model from: `https://github.com/ant-research/EasyTemporalPointProcess`.
SAHP: We add Self-Attention Hawkes Process (SAHP) Zhang et al. (2020) to the next event prediction comparison. SAHP uses self-attention mechanism in tranformers to define intensity function. We use the publicly available implementation of this model from: `https://github.com/ant-research/EasyTemporalPointProcess`.
RMTPP: Recurrent Marked Temporal Point Process (RMTPP) Du et al. (2016) defines a conditional intensity model based on RNN architecture. We include it in the next event prediction benchmark. We use the code available for this method in the public repository: `https://github.com/ant-research/EasyTemporalPointProcess`.

4 Generic hyperparameters for Next Observation Prediction Task

The following hyperparameters are applicable broadly across our forecasting experiments:

- For all models, we use Adam optimizer Kingma & Ba (2015).
- For all models, we apply exponential learning rate decay of 0.99 and perform gradient clipping using max l^2-norm=1.
- For all GRUwE configurations, we use the same architecture for the hidden to observation function $F_{out}(\mathbf{g}_{t,\Delta T})$: Linear(hidden_dim, target_dim).

5 Hyperparameters for Next Observation Prediction Task on USHCN

We keep batch size fixed to 50, the number of training epochs to 100, learning rate decay to 0.99, with gradient clipping and perform a hyperparameter search for each model as follows:

5.0.1 mTAND

For mTAND, we perform a grid search over time embedding dimension = $\{32, 64, 128\}$, latent state dimension =$\{8, 10, 16, 20\}$, number of reference points=$\{32, 64, 128\}$ and learning rate =$\{0.1, 0.05, 0.01, 0.001\}$. Of which, latent state dimension=8, number of reference points=32 and learning rate of 0.01 performs the best on the validation data.

5.0.2 GRU-D

For GRU-D, we perform a search over latent state dimension = $\{8, 10, 16, 20\}$ and learning rate = $\{0.1, 0.05, 0.01, 0.001\}$. We find that configuration with latent state dimension=20 and learning rate=0.01 performs best on the validation set.

5.0.3 CRU

Fixed hyperparameters for CRU are: variance activation for encoder='square', decoder='exp', transition='relu' encoder variance activation='square', decoder variance activation='exp', number of basis matrices=20, and the same encoder and decoder network architecture as used in Schirmer et al. (2022). We perform a search on latent state dimension=$\{8, 10, 16, 20\}$ and learning rate = $\{0.1, 0.05, 0.01, 0.001\}$. We report that the latent dimension=10 and learning rate=0.05 performs the best on validation set.

5.0.4 f-CRU

Fixed hyperparameters for f-CRU include: variance activation for encoder='square', decoder='exp', transition='relu' encoder variance activation='square', decoder variance activation='exp', number of basis matrices=20, and the same encoder and decoder network architecture as used in Schirmer et al. (2022). We perform a search on latent state dimension = $\{8, 10, 16, 20\}$ and learning rate = $\{0.1, 0.05, 0.01, 0.001\}$. We report that the latent dimension=10 and learning rate=0.05 performs the best on the validation set.

5.0.5 Latent ODE

We use Latent ODE model with ODE-RNN encoder. We perform a grid search on latent state dimension=$\{8, 10, 16, 20\}$, recognition network dimension=$\{16, 32, 64\}$, number of GRU units=$\{16, 32, 64\}$, number of generation layers=$\{2, 3\}$, number of recognition layers=$\{2, 3\}$ and learning rate= $\{0.1, 0.05, 0.01, 0.001\}$. The configuration that performs the best on validation split with latent state dimension, recognition network dimension, number of GRU units set to 20; learning rate of 0.01 and generation and recognition network layers set to 3.

5.0.6 ODE-RNN

For ODE-RNN, we use GRU as the RNN model and use the adjoint solver method implemented in the library: `https://github.com/rtqichen/torchdiffeq` for solving the ODEs in a differentiable manner. For ODE-RNN, we search over latent state dimension=$\{8, 10, 16, 20\}$ and the learning rates=$\{0.1, 0.05, 0.01, 0.001\}$. We find that the configuration of latent state dimension=20 and learning rate = 0.01 works the best on the validation set.

5.0.7 ContiFormer

We use the ContiFormer implementation released by the authors `https://github.com/microsoft/SeqML/tree/main/ContiFormer` in our implementation. Note that since USHCN has highest average sequence length, and ContiFormer is memory intensive, we can only fit a batch size of 4 samples in our GPU memory. Keeping other parameters fixed, we vary the latent state dimension = $\{8, 10, 16, 20\}$ and learning rate = $\{0.1, 0.05, 0.01, 0.001\}$. Our experiments show that latent state dimension=16 and learning rate=0.001 achieves the best performance on validation set.

5.0.8 GRU-Δ_t

For GRU-Δ_t, we search over latent state dimensions of the GRU =$\{8, 10, 16, 20\}$ and learning rates=$\{0.1, 0.05, 0.01, 0.005, 0.001\}$. We find latent state dimension=16 and learning rate=0.005 to be the best performing configuration.

5.0.9 RKN-Δ_t

We use the RKN-Δ_t implementation made available by the authors `https://github.com/ALRhub/rkn_share.git`. Our RKN-Δ_t implementation uses the same encoders and decoders architecture as the CRU model. Keeping other parameters fixed, we search over latent state dimensions = $\{8, 10, 16, 20\}$ and learning rates = $\{0.1, 0.05, 0.01, 0.005, 0.001\}$. Latent state dimension=20 and learning rate=0.001 results in the best performing model.

5.0.10 T-PatchGNN

We perform a grid search over learning rates = $\{0.1, 0.05, 0.01, 0.005, 0.001\}$, time and node embedding dimensions = $\{4, 8, 16\}$, number of patches=$\{2, 4\}$ (more number of patches results in GPU OOM issue), and latent state dimension = $\{4, 8, 10, 12, 16\}$, while fixing the number of heads in one transformer layer = number of transformer layers = 1. We find that the configuration with learning rate=0.001, time and node embedding dimension=8, number of patches=2, latent state dimension=16 results in the best validation MSE.

5.0.11 GraFITi

We perform a grid search over learning rates = $\{0.1, 0.05, 0.01, 0.005, 0.001\}$, latent state dimension = $\{4, 8, 16, 20, 32, 64\}$, number of layers = $\{1, 2, 4\}$ and number of attention heads = $\{1, 2, 4\}$. We report that the configuration with lr=0.01, latent state dimension=8, number of layer=2 and number of attention heads=1 results in the best validation MSE.

5.0.12 GRUwE

We perform a grid search over latent state dimensions=$\{8, 10, 16, 20\}$ (to be comparable to other baselines considered) with learning rates $\{0.1, 0.05, 0.01, 0.005, 0.001\}$. For USHCN, the best model configuration that maximizes validation prediction MSE uses learning rate=0.1 and latent state dimension=20.

5.0.13 HyperIMTS

We perform a grid search over learning rates = $\{0.1, 0.05, 0.01, 0.005, 0.001\}$, latent state dimension = $\{8, 16, 20, 32, 64, 128\}$, number of layers = $\{1, 2, 4\}$ and number of attention heads = $\{1, 2, 4\}$. We report that the configuration with lr=0.001, latent state dimension=32, number of layer=2 and number of attention heads=2 results in the best validation MSE.

6 Hyperparameters for Next Observation Prediction Task on Physionet

We keep the following hyperparameters constant across all methods: batch size=100, number of training epochs=100, learning rate decay=0.99 and gradient clipping enabled. Below are the model specific experiments we carried out.

6.0.1 mTAND

For mTAND, we perform a grid search over time embedding dimension = $\{32, 64, 128\}$, latent state dimension =$\{8, 10, 16, 20, 22, 24\}$, number of reference points=$\{32, 64, 128\}$ and learning rate = $\{0.1, 0.05, 0.01, 0.001\}$. Of which, time embedding dim=32, latent state dimension=22, number of reference points=64 and learning rate=0.01 performs the best on the validation data.

6.0.2 GRU-D

For GRU-D, we perform a search over latent state dimension = $\{8, 10, 16, 20, 22, 24, 32, 64\}$ and learning rate = $\{0.1, 0.05, 0.01, 0.001\}$. We find that configuration with latent state dimension=16 and learning rate=0.01 performs best on the validation set.

6.0.3 f-CRU

Fixed hyperparameters for f-CRU include: variance activation for encoder='square', decoder='exp', transition='relu' encoder variance activation='square', decoder variance activation='exp', number of basis matrices=20, and the same encoder and decoder network architecture as used in Schirmer et al. (2022). We perform a search on latent state dimension = $\{8, 10, 16, 20, 32, 64\}$ and learning rate = $\{0.1, 0.05, 0.01, 0.001\}$. We report that the latent dimension=16 and learning rate=0.001 performs the best on the validation set.

6.0.4 CRU

Fixed hyperparameters for CRU are: variance activation for encoder='square', decoder='exp', transition='relu' encoder variance activation='square', decoder variance activation='exp', number of basis matrices=20, and the same encoder and decoder network architecture as used in Schirmer et al. (2022). We perform a search on latent state dimension=$\{8, 10, 16, 20, 32, 64\}$ and learning rate = $\{0.1, 0.05, 0.01, 0.005, 0.001\}$. We report that the latent dimension=32 and learning rate=0.005 performs the best on validation set.

6.0.5 Latent ODE

We use Latent ODE model with ODE-RNN encoder. We perform a grid search on latent state dimension=$\{8, 10, 16, 20, 32, 64\}$, recognition network dimension=$\{16, 32, 64\}$, number of GRU units=$\{16, 32, 64\}$, number of generation layers=$\{2, 3\}$, number of recognition layers=$\{2, 3\}$ and learning rate= $\{0.1, 0.05, 0.01, 0.005, 0.001\}$. The configuration that performs the best on validation split with latent state dimension, recognition network dimension, number of GRU units set to 32; learning rate=0.005 and generation and recognition network layers set to 3.

6.0.6 ODE-RNN

For ODE-RNN, we search over latent state dimension=$\{8, 10, 16, 20, 32, 64\}$ and the learning rates=$\{0.1, 0.05, 0.01, 0.005, 0.001\}$. We find that the configuration of latent state dimension=16 and learning rate = 0.001 works the best on the validation set.

6.0.7 ContiFormer

For ContiFormer, we perform a search over the latent state dimension = $\{8, 16, 20, 32, 64\}$ and learning rate = $\{0.1, 0.05, 0.01, 0.001\}$. Our experiments show that latent state dimension=16 and learning rate=0.001 achieves the best performance on the validation set.

6.0.8 GRU-Δ_t

For GRU-Δ_t, we search over latent state dimensions of the GRU =$\{8, 10, 16, 20, 24, 32, 64\}$ and learning rates=$\{0.1, 0.05, 0.01, 0.005, 0.001\}$. We find latent state dimension=32 and learning rate=0.005 to be the best performing configuration.

6.0.9 RKN-Δ_t

Our RKN-Δ_t implementation uses the same encoders and decoders architecture as the CRU model. Keeping other parameters fixed, we search over latent state dimensions = $\{8, 10, 16, 20, 24, 32, 64\}$ and learning rates = $\{0.1, 0.05, 0.01, 0.005, 0.001\}$. Latent state dimension=32 and learning rate=0.001 results in the best performing model.

6.0.10 T-PatchGNN

We perform a grid search over learning rates = $\{0.1, 0.05, 0.01, 0.005, 0.001\}$, time and node embedding dimensions = $\{4, 8, 16\}$, number of patches=$\{5, 10, 20\}$, and latent state dimension = $\{4, 8, 16, 32, 64\}$, while fixing the number of heads in one transformer layer = number of transformer layers = 1. We find that the configuration with learning rate=0.001, time and node embedding dimension=8, number of patches=10, latent state dimension=8 results in the best validation MSE.

6.0.11 GraFITi

We perform a grid search over learning rates = $\{0.1, 0.05, 0.01, 0.005, 0.001\}$, latent state dimension = $\{4, 8, 10, 16, 20, 32, 64\}$, number of layers = $\{1, 2, 4\}$ and number of attention heads = $\{1, 2, 4\}$. We report that the configuration with lr=0.005, latent state dimension=64, number of layer=2 and number of attention heads=1 results in the best validation MSE.

6.0.12 GRUwE

We perform a search over learning rate=$\{0.1, 0.025, 0.05, 0.01, 0.005\}$, the hidden state dimensions= $\{10, 16, 20, 24, 32, 64\}$ (to be comparable to other models). For Physionet, we use learning rate=0.025 and latent state dimension=64.

6.0.13 HyperIMTS

We perform a grid search over learning rates = $\{0.1, 0.05, 0.01, 0.005, 0.001\}$, latent state dimension = $\{8, 16, 20, 32, 64, 128\}$, number of layers = $\{1, 2, 4\}$ and number of attention heads = $\{1, 2, 4\}$. We report

that the configuration with lr=0.005, latent state dimension=16, number of layer=2 and number of attention heads=4 results in the best validation MSE.

7 Hyperparameters for Next Observation Prediction Task on MIMIC-III-Small

We keep the following hyperparameters constant across all methods: batch size=100 (we reduce it for models if we face OOM issue), number of training epochs=100, learning rate decay=0.99 and gradient clipping enabled. Below are the model specific experiments we carried out.

7.0.1 mTAND

For mTAND, we perform a grid search over time embedding dimension = $\{32, 64, 128\}$, latent state dimension =$\{8, 16, 32, 64, 128\}$, number of reference points=$\{8, 32, 64, 128\}$ and learning rate = $\{0.1, 0.05, 0.01, 0.001, 0.0001\}$. Of which, time embedding dim=32, latent state dimension=128, number of reference points=8 and learning rate=0.0001 performs the best on the validation data.

7.0.2 GRU-D

For GRU-D, we perform a search over latent state dimension = $\{8, 10, 16, 32, 64, 128\}$ and learning rate = $\{0.1, 0.05, 0.01, 0.001\}$. We find that configuration with latent state dimension=64 and learning rate=0.001 performs best on the validation set.

7.0.3 f-CRU

Fixed hyperparameters for f-CRU include: variance activation for encoder='square', decoder='exp', transition='relu' encoder variance activation='square', decoder variance activation='exp', number of basis matrices=20, and the same encoder and decoder network architecture as used in Schirmer et al. (2022). We perform a search on latent state dimension = $\{8, 10, 16, 20, 32, 64\}$ and learning rate = $\{0.1, 0.05, 0.01, 0.001, 0.0001\}$. We report that the latent dimension=64 and learning rate=0.0001 performs the best on the validation set.

7.0.4 CRU

Fixed hyperparameters for CRU are: variance activation for encoder='square', decoder='exp', transition='relu' encoder variance activation='square', decoder variance activation='exp', number of basis matrices=20, and the same encoder and decoder network architecture as used in Schirmer et al. (2022). We perform a search on latent state dimension=$\{8, 10, 16, 20, 32, 64\}$ and learning rate = $\{0.1, 0.05, 0.01, 0.005, 0.001\}$. We report that the latent dimension=32 and learning rate=0.005 performs the best on validation set.

7.0.5 Latent ODE

We use Latent ODE model with ODE-RNN encoder. We perform a grid search on latent state dimension=$\{8, 10, 16, 20, 32, 64\}$, recognition network dimension=$\{16, 32, 64\}$, number of GRU units=$\{16, 32, 64\}$, number of generation layers=$\{2, 3\}$, number of recognition layers=$\{2, 3\}$ and learning rate= $\{0.1, 0.05, 0.01, 0.005, 0.001\}$. The configuration that performs the best on validation split with latent state dimension, recognition network dimension, number of GRU units set to 32; learning rate=0.001 and generation and recognition network layers set to 3.

7.0.6 ODE-RNN

For ODE-RNN, we search over latent state dimension=$\{8, 10, 16, 20, 32, 64\}$ and the learning rates=$\{0.1, 0.05, 0.01, 0.005, 0.001, 0.0001\}$. We find that the configuration of latent state dimension=64 and learning rate = 0.0001 works the best on the validation set.

7.0.7 ContiFormer

For ContiFormer, we perform a search over the latent state dimension = $\{8, 16, 20, 32, 64\}$ and learning rate = $\{0.1, 0.05, 0.01, 0.001\}$. Our experiments show that latent state dimension=16 and learning rate=0.001 achieves the best performance on the validation set.

7.0.8 GRU-Δ_t

For GRU-Δ_t, we search over latent state dimensions of the GRU =$\{8, 10, 16, 20, 24, 32, 64\}$ and learning rates=$\{0.1, 0.05, 0.01, 0.005, 0.001\}$. We find latent state dimension=32 and learning rate=0.005 to be the best performing configuration.

7.0.9 RKN-Δ_t

Our RKN-Δ_t implementation uses the same encoders and decoders architecture as the CRU model. Keeping other parameters fixed, we search over latent state dimensions = $\{8, 10, 16, 20, 24, 32, 64\}$ and learning rates = $\{0.1, 0.05, 0.01, 0.005, 0.001, 0.0001\}$. Latent state dimension=64 and learning rate=0.0001 results in the best performing model.

7.0.10 T-PatchGNN

We perform a grid search over learning rates = $\{0.1, 0.05, 0.01, 0.005, 0.001, 0.0001\}$, time and node embedding dimensions = $\{4, 8, 16\}$, number of patches=$\{5, 10, 20\}$, and latent state dimension = $\{4, 8, 16, 32, 64\}$, while fixing the number of heads in one transformer layer = number of transformer layers = 1. We find that the configuration with learning rate=0.0001, time and node embedding dimension=16, number of patches=10, latent state dimension=16 results in the best validation MSE.

7.0.11 GraFITi

We perform a grid search over learning rates = $\{0.1, 0.05, 0.01, 0.005, 0.001\}$, latent state dimension = $\{4, 8, 10, 16, 20, 32, 64\}$, number of layers = $\{1, 2, 4\}$ and number of attention heads = $\{1, 2, 4\}$. We report that the configuration with lr=0.005, latent state dimension=64, number of layer=2 and number of attention heads=1 results in the best validation MSE.

7.0.12 GRUwE

We perform a search over learning rate=$\{0.1, 0.025, 0.05, 0.01, 0.005\}$, the hidden state dimensions= $\{10, 16, 20, 24, 32, 64\}$ (to be comparable to other models). For MIMIC-III-Small, we use the configuration that results in the best validation MSE: learning rate=0.001 and latent state dimension=32.

7.0.13 HyperIMTS

We perform a grid search over learning rates = $\{0.1, 0.05, 0.01, 0.005, 0.001\}$, latent state dimension = $\{8, 16, 20, 32, 64, 128\}$, number of layers = $\{1, 2, 4\}$ and number of attention heads = $\{1, 2, 4\}$. We report that the configuration with lr=0.005, latent state dimension=32, number of layer=2 and number of attention heads=4 results in the best validation MSE.

8 Hyperparameters for Next Observation Prediction Task on MIMIC-III-Large

We keep the following hyperparameters constant across all methods: batch size=1 (to be able to handle the longer sequences in the MIMIC-III dataset within GPU memory constraints), number of training epochs=20, learning rate decay=0.99 and gradient clipping enabled. Below are the model specific experiments we carried out.

8.0.1 mTAND

Based on MIMIC-III experiments in Shukla & Marlin (2021), we keep the following hyperparameters fixed: time embedding dimension=128. We perform grid search on the hidden state dimension = $\{16, 32, 64\}$, encoder hidden dimension = $\{16, 32, 64\}$, the number of reference points = $\{64, 95\}$ and the learning rates=$\{0.01, 0.005, 0.001\}$. Note that for both hidden state dimensions as 64 and number of reference points as 95, we hit the memory limit on our GPU for batch size=1. Nonetheless, the resulting number of parameters (=174K) for this configuration is higher than that of our proposed model. Our validation results show that latent state dimension=64, number of reference points=95 and learning rate=0.001 performs the best across all combinations.

8.0.2 GRU-D

We perform grid search over hidden state dimension=$\{16, 32, 64\}$ and learning rates=$\{0.01, 0.005, 0.001\}$. We report that hidden state=32 and learning rate=0.001 performs the best on validation set and use it to report the final results.

8.0.3 Latent ODE

We use Latent ODE model with ODE-RNN encoder. We perform a grid search on latent state dimension=$\{16, 32, 64\}$, recognition network dimension=$\{16, 32, 64\}$, number of GRU units=$\{16, 32, 64\}$, number of generation layers=$\{2, 3\}$, number of recognition layers=$\{2, 3\}$ and learning rate=

$\{0.01, 0.005, 0.001\}$. The configuration that performs the best on validation split with latent state dimension, recognition network dimension, number of GRU units set to 32; learning rate of 0.001 and generation and recognition network layers set to 3. Other hyperparameters that were kept fixed are: batch size=1, learning rate decay=0.99 with gradient clipping.

8.0.4 f-CRU

We perform a grid search over the latent state dimensions= $\{16, 32, 64\}$ and learning rates=$\{0.01, 0.005, 0.001\}$. We set latent observation dimension as half the size of latent state dimension. Number of basis matrices = 20, and Gradient clipping enabled. Encoder consists of 3 $\times$(FullyConnected(50) + ReLU + Layer normalization) followed by linear output for latent observation and output; square activation for latent observation variance. Decoder consists of 3 $\times$ (FullyConnected(50) + ReLU + Layer normalization) followed by a linear output. Decoder output variance consists of (FullyConnected(50) + ReLU + Layer normalization) followed by linear output and square activation. Activation function for transition function is ReLU. After performing the grid search, the best configuration of hyperparameters are: latent state dimension=64, and learning rate=0.001.

8.0.5 CRU

Fixed hyperparameters for CRU are: variance activation for encoder='square', decoder='square', transition='relu', number of basis matrices=20, and the same encoder and decoder network architecture used in f-CRU (above). We perform a search on latent state dimension=$\{16, 32, 64\}$ and learning rate = $\{0.1, 0.01, 0.001, 0.0001\}$. We report that the latent dimension=32 and learning rate=0.0001 performs the best on validation set.

8.0.6 ODE-RNN

For ODE-RNN, we search over latent state dimension=$\{16, 32, 64\}$ and the learning rates=$\{0.1, 0.05, 0.01, 0.005, 0.001\}$. We find that the configuration of latent state dimension=32 and learning rate = 0.005 works the best on the validation set.

8.0.7 ContiFormer

For ContiFormer, we perform a search over the latent state dimension = $\{16, 32, 64\}$ and learning rate = $\{0.1, 0.05, 0.01, 0.001\}$. Our experiments show that latent state dimension=64 and learning rate=0.001 achieves the best performance on the validation set.

8.0.8 GRU-Δ_t

For GRU-Δ_t, we search over latent state dimensions of the GRU =$\{16, 32, 64\}$ and learning rates=$\{0.1, 0.05, 0.01, 0.005, 0.001\}$. We find latent state dimension=16 and learning rate=0.001 to be the best performing configuration.

8.0.9 RKN-Δ_t

Our RKN-Δ_t implementation uses the same encoders and decoders architecture as the CRU model. Keeping other parameters fixed, we search over latent state dimensions = $\{16, 32, 64\}$ and learning rates = $\{0.001, 0.0005, 0.0001, 0.00005\}$. Note that we search over smaller values of the learning rate because, the model would not converge for higher ones (we get "NaN" during optimization for higher rate). Latent state dimension=32 and learning rate=0.00005 results in the best performing model.

8.0.10 T-PatchGNN

We perform a grid search over learning rates = $\{0.1, 0.05, 0.01, 0.005, 0.001\}$, time and node embedding dimensions = $\{4, 8, 16\}$, number of patches=$\{2, 4\}$ (more number of patches results in GPU OOM issue), and latent state dimension = $\{4, 8, 10, 12\}$, while fixing the number of heads in one transformer layer = number of transformer layers = 1. We find that the configuration with learning rate=0.001, time and node embedding dimension=20, number of patches=2, latent state dimension=12 results in the best validation MSE.

8.0.11 GraFITi

We perform a grid search over learning rates = $\{0.1, 0.05, 0.01, 0.005, 0.001\}$, latent state dimension = $\{16, 32, 64\}$, number of layers = $\{1\}$ (more number of layers on MIMIC-III causes OOM) and number of

attention heads = {1}. We report that the configuration with lr=0.005, latent state dimension=64, number of layer=1 and number of attention heads=1 results in the best validation MSE.

8.0.12 GRUwE

After searching over hidden state=$\{10, 16, 20\}$ and learning rates=$\{0.1, 0.05, 0.01, 0.005, 0.001\}$. For the prediction tasks, we find the combination of 16 and 0.001 perform the best.

8.0.13 HyperIMTS

For HyperIMTS, we were unable to run experiments on the MIMIC-III Large dataset because even the smallest tested configuration (batch size = 1, latent dimension = 8, number of layers = 1, number of attention heads = 2) consistently triggered GPU memory errors during training. It is very likely due to long sequences in the MIMIC-III Large dataset as reported in Table 5.

9 Hyperparameters for Event Prediction task

We perform a grid search to tune the hyperparameters for the event prediction models: GRUwE, NHP, ATTNHP, THP and RMTPP. For RNN-based models (i.e., GRUwE, NHP, RMTPP), hidden size, learning rate and batch size are the relevant hyperparameters. For Attention-based models (i.e., ATTNHP, THP, SAHP), we optimize hidden size, learning rate, batch size, number of attention layers and embedding size. For all our experiments, we use Adam optimizer during training.

Table 6: Grid search configurations for hyperparameter tuning

Model Type	**Hyperparameter**	**Values**
RNN-based (NHP, RMTPP, GRUwE)	hidden size	{16, 32, 64}
	learning tate	{1e-1, 5e-2, 1e-2, 5e-3, 1e-3}
	batch size	{32, 64, 128, 256}
Attention-based (ATTNHP, THP)	hidden Size	{16, 32, 64}
	embedding size	{4, 8, 16}
	num. layers	{1, 2, 3}
	learning rate	{1e-1, 5e-2, 1e-2, 5e-3, 1e-3}
	batch size	{32, 64, 128, 256}

The grid search values for each parameter are reported in Table 6. For each dataset, we perform an independent hyperparameter search and train the model for up to 30 epochs with early stopping based on validation log-likelihood. We select the model configuration that achieves the highest validation log-likelihood.

10 Rank-based analysis for next event prediction.

We use the rank metrics as described in Table 7 to report the average rank statistic in the main results of our paper.

Table 7: Model performance comparison for the next event prediction on the Taxi, Retweet, StackOverflow, and Amazon datasets. Lower rank means better model for RMSE and ER metrics.

	Taxi		**Retweet**		**StackOverflow**		**Amazon**	
Model	RMSE (Rank)	ER (Rank)	RMSE (Rank)	ER (Rank)	RMSE (Rank)	ER (Rank)	RMSE (Rank)	ER (Rank)
FullyNN	0.373 (7)	N.A.	**21.92 (1)**	N.A.	1.375 (6)	N.A.	0.615 (5)	N.A.
NHP	**0.369 (1)**	9.22 (3)	22.32 (5)	**40.25 (1)**	1.369 (2)	55.78 (4)	0.612 (2)	68.30 (5)
A-NHP	0.370 (4)	11.42 (6)	22.28 (3)	41.05 (4)	1.370 (4)	55.51 (2)	0.612 (2)	**65.65 (1)**
THP	**0.369 (1)**	8.85 (2)	22.32 (5)	**40.25 (1)**	**1.368 (1)**	55.60 (3)	0.612 (2)	66.72 (2)
SAHP	0.372 (6)	9.75 (4)	22.40 (7)	41.60 (5)	1.375 (6)	56.10 (5)	0.619 (6)	67.70 (4)
RMTPP	0.370 (4)	9.86 (5)	22.31 (4)	44.10 (6)	1.370 (4)	57.50 (6)	0.634 (7)	73.66 (6)
GRUwE	**0.369 (1)**	**8.58 (1)**	22.21 (2)	40.81 (3)	1.369 (2)	**55.34 (1)**	**0.611 (1)**	67.24 (3)

11 Computational Cost Analysis

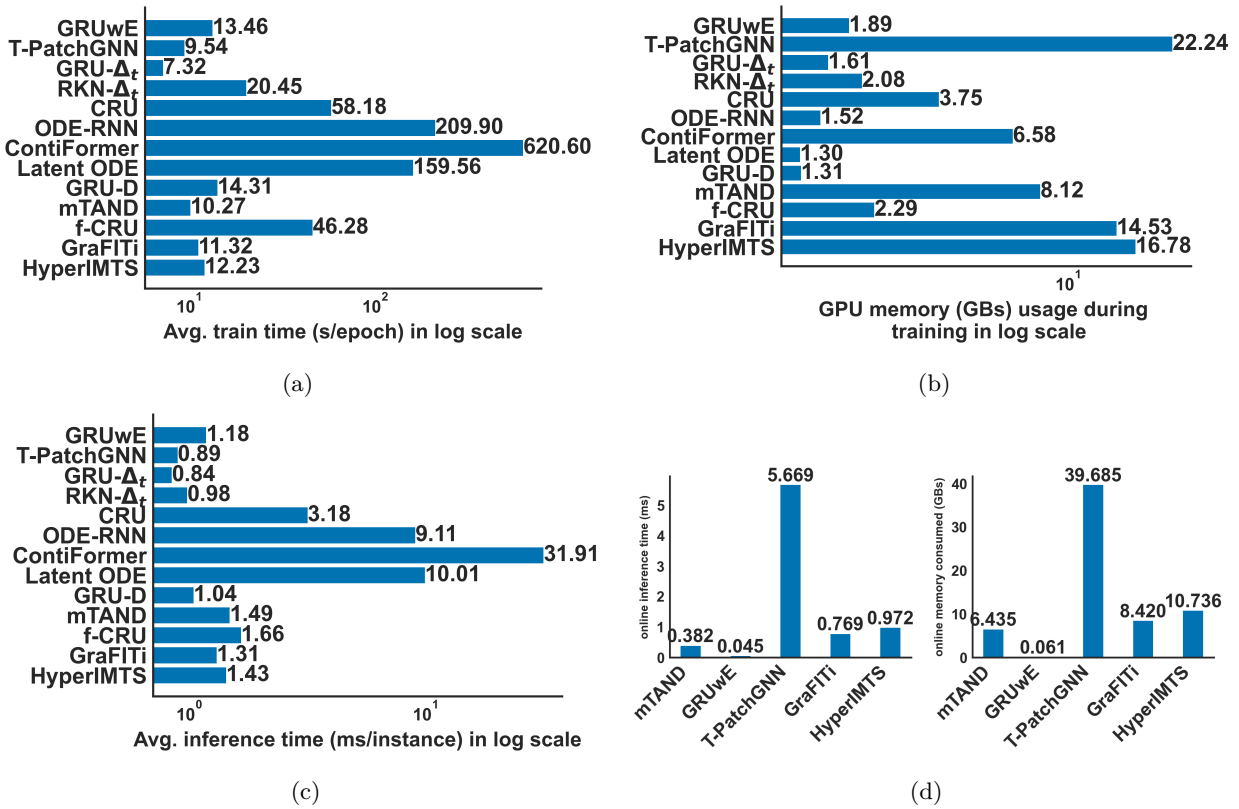

Figure 6: Computational cost analysis on the Physionet dataset. (**a**) Compares the average train time per epoch in seconds. (**b**) Peak GPU memory usage in GBs during training. (**c**) Average inference time in milliseconds per instance. (**d**) Comparison of the inference time (**left**) and memory consumption (**right**) in an online deployment.

We provide a comprehensive comparison of the computational complexity across all models investigated in our study in the Figure 6. We evaluate and contrast the training times, inference times, and peak GPU memory usage during training for each model when performing next observation prediction task on the Physionet dataset. The average train and inference times are computed by taking the average across multiple epochs and samples. Our analysis reveals a clear trend in terms of the train time. We note that methods (ContiFormer, ODE-RNN, Latent ODE) that rely on numerical solvers exhibit the longest training times, followed by models (CRU, f-CRU, RKN-Δ_t) that assume linear dynamics. Recurrent models (GRUwE, GRU-D, GRU-Δ_t) demonstrate moderate training times. Lastly, models that can be parallelized in the time dimension (mTAND, T-PatchGNN, GraFITi, HyperIMTS) are the fastest to train. However, it is crucial to note that the models with the fastest training times (mTAND, T-PatchGNN, GraFITi, HyperIMTS) come with a significantly higher memory requirement as illustrated in Figure 6b.

Having trained the time series model on retrospective EHR data, our primary goal is to deploy it as an early warning system to prevent adverse patient conditions in the ICU. This model operates in an inherently online context, characterized by a continuous stream of (near) real-time data. This data stream includes critical patient information such as vital signs and medication administration records, which the deployed model processes continuously. To simulate this online environment, we use the Physionet dataset, streaming observations from 100 randomly selected patients in an online manner. The models are evaluated based on total inference time and peak GPU memory usage during inference. In our analysis, we compare GRUwE with models that offer the best train times and are among the top performing models in next observation prediction task: mTAND, GraFITi and T-PatchGNN. We observe that since mTAND, GraFITi, T-PatchGNN and HyperIMTS do not have a Markovian state representation, it needs to buffer the past observations to make the inference. This results in higher inference cost both in terms of time and memory. Moreover, these

costs grows over time. In contrast, models that consists of Markov state representation such as GRUwE, are independent of the past observations thus, maintaining a constant, low time and memory requirement.

12 Computing Infrastructure

We used one server machine to deploy the experiments reported in the paper. This machine is equipped with 100GB memory, one NVIDIA L40S GPU, with Intel Xeon Platinum 8462Y+ @ 2.80 GHz processor and 16 CPU cores.